J. Fluid Mech. (2001), *vol.* 434, *pp.* 301–335. Printed in the United Kingdom

© 2001 Cambridge University Press

Interaction of water waves with three-dimensional periodic topography

By R. PORTER[1] AND D. PORTER[2]

[1]School of Mathematics, University of Bristol, Bristol, BS8 1TW, UK

[2]Department of Mathematics, The University of Reading, PO Box 220, Whiteknights, Reading, RG6 6AX, UK

(Received 27 June 2000 and in revised form 25 October 2000)

The scattering and trapping of water waves by three-dimensional submerged topography, infinite and periodic in one horizontal coordinate and of finite extent in the other, is considered under the assumptions of linearized theory. The mild-slope approximation is used to reduce the governing boundary value problem to one involving a form of the Helmholtz equation in which the coefficient depends on the topography and is therefore spatially varying.

Two problems are considered: the scattering by the topography of parallel-crested obliquely incident waves and the propagation of trapping modes along the periodic topography. Both problems are formulated in terms of 'domain' integral equations which are solved numerically.

Trapped waves are found to exist over any periodic topography which is 'sufficiently' elevated above the unperturbed bed level. In particular, every periodic topography wholly elevated above that level supports trapped waves. Fundamental differences are shown to exist between these trapped waves and the analogous Rayleigh–Bloch waves which exist on periodic gratings in acoustic theory.

Results computed for the scattering problem show that, remarkably, there exist zeros of transmission at discrete wavenumbers for any periodic bed elevation and for all incident wave angles. One implication of this property is that total reflection of an incident wave of a particular frequency will occur in a channel with a single symmetric elevation on the bed. The zeros of transmission in the scattering problem are shown to be related to the presence of a 'nearly trapped' mode in the corresponding homogeneous problem.

The scattering of waves by multiple rows of periodic topography is also considered and it is shown how Bragg resonance – well-established in scattering of waves by two-dimensional ripple beds – occurs in modes other than the input mode.

1. Introduction

The interaction of waves with periodic structures has been a subject of interest in many branches of applied mathematics including solid-state physics, electromagnetic wave propagation and fluid dynamics. The present study is set in the context of water waves, although the governing equations that will be used to describe the fluid motion have physical relevance in other settings such as electromagnetic theory, where this particular problem may be thought of as the propagation of waves within a medium having periodic impedance.

In the two-dimensional problem of the scattering of water waves by topography

having periodic elevation (so-called ripple beds), it is well known that amplification can occur in the modulus of the reflection coefficient as the number of ripples is increased for certain intervals of the wavenumber, to the extent that almost total reflection can be attained. This example of Bragg resonance has been the subject of many investigations, recent contributions having been made by Mei (1985), Kirby (1986), Guazzelli, Rey & Belzons (1992), O'Hare & Davies (1992) and Chamberlain & Porter (1995).

In three dimensions, periodic geometrical arrangements which extend infinitely in one of the horizontal directions can lead to the existence of a persistent localized wave field propagating along the structure in the absence of external excitation. Such trapping wave modes are often referred to as edge waves or Rayleigh–Bloch waves. In the context of water waves, Rayleigh–Bloch wave solutions have been found for several families of periodic geometries which extend uniformly throughout water of constant depth. This allows the depth dependence to be factorized from the governing potential and the resulting two-dimensional problem is governed by the Helmholtz equation with each obstacle in the periodic array represented by its cross-section and having a Neumann condition placed upon its boundary to represent the no-flow condition. Again, this problem has applications in many other physical settings including optics and acoustics as well as those previously mentioned. Evans & Linton (1993) computed the Rayleigh–Bloch wave solutions for an infinite array of parallel plates each perpendicular to the array whilst Rayleigh–Bloch waves along arrays of rectangular blocks and circular cylinders were subsequently investigated by Evans & Fernyhough (1995) and McIver, Linton & McIver (1998) respectively. More recently, Porter & Evans (1999) considered the Rayleigh–Bloch waves supported by periodic arrays of identical vertical cylinders having an arbitrary cross-section, using an integral equation formulation based on the use of the appropriate Green's function. They showed that, providing each of the cylinders is symmetric about a plane perpendicular to the plane containing the array, the generally complex system of algebraic equations reduced to a system for which the determinant is real and that Rayleigh–Bloch solutions corresponded to the vanishing of this real determinant for certain choices of real wavenumber.

Subsequently, however, and in the light of the results in the present work, one of the authors (R. Porter) has shown numerically that for cylinders which do not possess symmetry about this plane perpendicular to the array, solutions also appear to exist, even though they are now determined by locating zeros of a complex-valued determinant which is a function of the real wavenumber. Porter & Evans (1999) also showed that there is a simple connection between Rayleigh–Bloch waves and the trapped modes about multiple periodically spaced cylinders spanning a parallel waveguide having either Neumann or Dirichlet conditions on the walls of the waveguide. Simultaneous work of Utsunomiya & Eatock Taylor (1999) demonstrated, using circular cylinders, that these trapped modes in a waveguide are closely related to the near-trapped modes about a corresponding configuration of cylinders in open sea, as described by Maniar & Newman (1997). Thus Rayleigh–Bloch solutions are not only interesting in their own right; they also provide significant information about the solutions to other problems.

This paper is concerned with the interaction of linearized surface gravity water waves with three-dimensional periodic topography. More specifically, the topography is periodic within an infinite strip outside which the water is of constant equilibrium depth h_0. Two distinct problems arise from this situation. The first is the trapping problem discussed in the preceding paragraphs in which the possibility of a localized

solution, or trapped mode, is considered in the absence of any external excitation. The justification for seeking such a solution comes from consideration of wavenumbers k_0 related to the quiescent depth h_0 through the linearized dispersion relation for water waves which are below the cut-off β, where β is a wavenumber relating the phase of the solution from a point in one period of the array to the corresponding point in the adjacent period. Thus for values of $k_0 < \beta$ it can be shown that the solution, if it exists, will decay exponentially away from the strip containing the topography and will, in general, propagate energy along the strip.

The second part of the paper considers the scattering problem for the periodic topography when a monochromatic wave is obliquely incident on the array. In the scattering problem $k_0 > \beta$, since $\beta = k_0 \sin\theta_0$ is now defined as the component of the incident wavenumber in the direction parallel to the infinite array. The periodic array acts as a diffraction grating and thus, for a given incident wavenumber and angle, there will exist a finite set of discrete propagating modes with certain wavenumbers. Similar studies of diffraction of waves by three-dimensional periodic structures have been carried out, though these have been mainly concerned with geometrical structures having uniform cross-section throughout the depth. For example, see Linton & Evans (1993) and references therein.

A wide-spacing approximation is applied to the scattering of waves by multiple rows of periodic topography. Since there is, for a large enough wavenumber, a number of reflected and transmitted modes generated by a wave incident on a single strip of topography, there exists the possibility of Bragg resonance in a number of modes for multiple rows of topography. It is shown that resonance not only occurs at the wavelengths expected by analogy with Bragg resonance in the two-dimensional case, where one considers the interaction of a single mode with the periodic bed, but also at other wavenumbers where the resonance is caused by the interaction between the bed and multiple propagating modes.

In both the trapping problem and the scattering problem the method of solution is based upon the use of the mild-slope approximation to reduce the three-dimensional problem in an infinite strip containing just one typical period of topography in the infinite array to a two-dimensional problem. The mild-slope approximation involves applying an averaging procedure to the vertical structure of the wave field and integrating the depth variable out of the solution. As a result, the reduced problem satisfies the two-dimensional Helmholtz equation in the strip with a variable coefficient which contains the information about the topography. Outside the region of varying topography, this coefficient is constant and equal to k_0^2.

Rather than the using the mild-slope equation, which was originally derived independently by Berkhoff (1973, 1976) and Smith & Sprinks (1975), we employ the so-called modified mild-slope equation developed by Chamberlain & Porter (1995). As those authors showed, the modified version of the equation is more successful than its predecessor in modelling Bragg resonance for two-dimensional ripple beds. Indeed, it gives values for the reflected wave amplitude at resonance which correspond very closely with the experimental data of Davies & Heathershaw (1984). The reason for the superiority of the modified mild-slope equation in this context is easy to identify: the equation contains additional terms, one of which is proportional to $\nabla^2 h$, where h is the local quiescent depth, and for ripple beds the contribution of this term is comparable in magnitude to that of terms in the original mild-slope equation.

The integral equations that result from the use of the modified mild-slope equation are solved numerically using a simple, but robust, discretization which gives good accuracy for relatively coarse discretizations. A range of results for the trapping and

scattering problems is given at the end of the respective sections. One of the most significant is the existence of frequencies at which incident waves are totally reflected by the submerged periodic topography. It is shown that these are frequencies at which waves are 'nearly trapped' over the topography. This phenomenon therefore forms a connection between the scattering and trapping problems.

2. Formulation

Although the scattering and trapping problems ultimately have to be considered separately, a common formulation is possible initially.

The topography may be described by using Cartesian coordinates with the x- and y-axes lying in the mean free surface and z directed vertically upwards. The bed elevation is then given by $z = -h(x, y)$ where $h(x, y)$ is a continuous function and is such that $h(x, y) = h_0$, a constant, in $|x| \geqslant a$, $-\infty < y < \infty$. In $|x| < a$, we suppose that the topography is periodic in the y-direction with period $2d$ and therefore set $h(x, y + 2jd) = h(x, y)$ for $j = \pm 1, \pm 2, \ldots$. The arrangement described does not preclude the existence of regions within $|x| < a$ where $h(x, y) = h_0$.

With the usual assumptions of linearized water wave theory in force, that the fluid is incompressible and inviscid and its motion is irrotational, there exists a velocity potential which, with a time-harmonic component imposed, can be written as $\mathrm{Re}\{\Phi(x, y, z)\mathrm{e}^{-\mathrm{i}\omega t}\}$, where the angular frequency ω is given. Given the periodicity of the topography, we seek the time-independent complex potential $\Phi(x, y, z)$ which satisfies the relation

$$\Phi(x, y + 2jd, z) = \mathrm{e}^{2\mathrm{i}j\beta d}\Phi(x, y, z), \quad j = \pm 1, \pm 2, \ldots, \tag{2.1}$$

where the rôle of the real parameter β depends on the particular problem being considered, as will become clear in due course; for the present we may assume that β is assigned. As an alternative to (2.1), we may write the potential Φ in the form

$$\Phi(x, y, z) = \mathrm{e}^{\mathrm{i}\beta y}\Psi(x, y, z) \tag{2.2}$$

where $\Psi(x, y, z)$ is periodic in y with period $2d$.

Equation (2.1) provides the continuation of Φ from any domain of width $2d$ in the y-direction to the whole flow field. Thus, we only need to determine Φ in one such domain, which we choose to be defined by $(x, y) \in S$, $-h(x, y) \leqslant z \leqslant 0$, where

$$S = \{(x, y) : -\infty < x < \infty, -d \leqslant y \leqslant d\}.$$

We shall eventually need to distinguish those points of S which correspond to the region of varying depth and for this purpose it is convenient to introduce subdomains

$$S_h = \{(x, y) \in S : h(x, y) \neq h_0\}, \quad S_0 = S \backslash S_h.$$

We note that S_h need not be simply connected.

Within the chosen domain, the function Φ is required to satisfy the standard equations of linearized wave theory, namely

$$\nabla^2\Phi = 0, \quad -h(x, y) \leqslant z \leqslant 0, \ (x, y) \in S, \tag{2.3}$$

where $\nabla = (\partial/\partial x, \partial/\partial y, \partial/\partial z)$,

$$\Phi_z - \nu\Phi = 0, \quad z = 0, \ (x, y) \in S, \tag{2.4}$$

where $\nu = \omega^2/g$, and

$$\Phi_z + \nabla h \cdot \nabla\Phi = 0, \quad z = -h(x, y), \ (x, y) \in S. \tag{2.5}$$

In addition, the coupled boundary conditions

$$\left.\begin{aligned}\Phi(x,d,z) &= \mathrm{e}^{2\mathrm{i}\beta d}\Phi(x,-d,z),\\ \Phi_y(x,d,z) &= \mathrm{e}^{2\mathrm{i}\beta d}\Phi_y(x,-d,z),\end{aligned}\right\} \quad -h(x,d)\leqslant z\leqslant 0, \quad -\infty<x<\infty, \tag{2.6}$$

follow from (2.1).

To complete the set of equations which define Φ requires specification of its behaviour as $|x|\to\infty$ in $S\times[-h,0]$, obtained by solving the existing equations in $|x|>a$, where the bed is flat and the quiescent depth is h_0. This is easily accomplished by separation of variables. We first note that (2.2) implies

$$\Phi(x,y,z)=\sum_{m=-\infty}^{\infty}\psi_m(x,z)\mathrm{e}^{\mathrm{i}\beta_m y},$$

where

$$\beta_m=\beta+m\pi/d, \quad m\in\mathbb{Z}, \tag{2.7}$$

and, in particular, $\beta_0=\beta$. The set of functions $\mathrm{e}^{\mathrm{i}\beta_m y}$ $(m\in\mathbb{Z})$ is orthonormal on the interval $[-d,d]$, with weight $2d$, and is complete. This expansion necessarily satisfies (2.6) and imposing (2.3), (2.4) and (2.5) readily leads to the set of separation solutions

$$\left.\begin{aligned}\Phi_{m,0}(x,y,z) &= \frac{\cosh\{k_0(z+h_0)\}}{\cosh(k_0h_0)}\,\mathrm{e}^{\pm\gamma_m x+\mathrm{i}\beta_m y}, \quad m\in\mathbb{Z},\\ \Phi_{m,n}(x,y,z) &= \frac{\cos\{k_n(z+h_0)\}}{\cos(k_nh_0)}\,\mathrm{e}^{\pm\delta_{m,n}x+\mathrm{i}\beta_m y}, \quad m\in\mathbb{Z},\ n\in\mathbb{N}.\end{aligned}\right\} \tag{2.8}$$

Here we have used the notation

$$\gamma_m=(\beta_m^2-k_0^2)^{1/2}, \quad \delta_{m,n}=(\beta_m^2+k_n^2)^{1/2},$$

and written k_0 to denote the real, positive root of the dispersion relation

$$k_0\tanh(k_0h_0)=\nu \tag{2.9}$$

and k_n, for $n\in\mathbb{N}$, to denote the real, positive roots of

$$k_n\tan(k_nh_0)=-\nu$$

arranged so that $k_{n+1}>k_n$.

It is now clear that propagating waves in $|x|\gg a$ are possible only if $-k_0<\beta_m<k_0$ for at least one value of m. We shall later arrange the notation to ensure that, if there is only one such wave, it corresponds to $m=0$, a convention which simplifies the condition that propagating waves can exist in the far field to $-k_0<\beta<k_0$. To enumerate all possible far field modes we introduce the non-negative integers r and s such that

$$\beta_{-r-1}<-k_0<\beta_{-r}\leqslant\beta_s<k_0<\beta_{s+1}. \tag{2.10}$$

If we now define

$$\gamma_m=-\mathrm{i}\alpha_m, \quad \alpha_m=(k_0^2-\beta_m^2)^{1/2}, \quad -r\leqslant m\leqslant s,$$

we see from (2.8) that, in the most general case, the behaviour of Φ for large $|x|$ may be expressed in the form

$$\Phi(x,y,z)\sim\frac{\cosh\{k_0(z+h_0)\}}{\cosh(k_0h_0)}\sum_{m=-r}^{s}\{A_m^{\pm}\mathrm{e}^{\mp\mathrm{i}\alpha_m x}+B_m^{\pm}\mathrm{e}^{\pm\mathrm{i}\alpha_m x}\}\mathrm{e}^{\mathrm{i}\beta_m y}, \quad x\to\pm\infty. \tag{2.11}$$

If (2.10) holds we have posed a scattering problem in which the amplitudes $A_m^{\pm}$ of the incoming waves must be prescribed and the amplitudes $B_m^{\pm}$ of the outgoing waves are to be determined.

Otherwise, if $|\beta_m| > k_0$ for all $m \in \mathbb{Z}$, then all of the modes in (2.8) are evanescent in x and the condition $\Phi \to 0$ as $|x| \to \infty$ replaces (2.11). The boundary value problem is now homogeneous and non-trivial solutions, if they exist, represent waves propagating parallel to the y-axis which are trapped over the topography.

Either way, the problem as it stands is formidable and we therefore seek to approximate its solution by invoking the mild-slope approximation. This has the effect of reducing the dimension of the problem by approximating the vertical motion of the fluid. We thus let

$$\Phi(x, y, z) \approx \frac{\cosh\{k(z+h)\}}{\cosh(kh)}\,\phi(x, y) \tag{2.12}$$

in which $k(h(x, y))$ denotes the positive, real root of the local dispersion relation

$$k \tanh(kh) = \nu,$$

where the depth is $h(x, y)$. Chamberlain & Porter (1995) implemented the approximation (2.12) by using a variational principle having (2.3), (2.4) and (2.5) as its natural conditions, a procedure which replaces those equations by the single modified mild-slope equation

$$\left.\begin{aligned} \nabla\cdot(u_0\nabla\phi) + v_0\phi = 0, \quad (x, y) \in S, \\ v_0 = k^2u_0 + u_1\nabla^2 h + u_2(\nabla h)^2. \end{aligned}\right\} \tag{2.13}$$

(The removal of z from the proceedings means that $\nabla = (\partial/\partial x, \partial/\partial y)$ from this point.) The positive-valued function $u_0(h(x, y))$ is given by

$$u_0 = \operatorname{sech}^2 kh(2kh + \sinh 2kh)/4k.$$

The other coefficients in (2.13), u_1 and u_2, need not be given explicitly here, as they will shortly be subsumed into other terms. We remark, however, that (2.13) reduces to the simpler but often less accurate mild-slope equation due originally to Berkhoff (1972, 1976) if the terms u_1 and u_2 are set to zero. A further simplification occurs in the long wave limit $kh \ll 1$ when (2.13) reduces to the familiar shallow water equation in which $u_0 = h$ and $v_0 = k^2h = \nu$. Indeed, (2.13) extends the shallow water equation to all kh. We assume that ∇h is continuous. If this is not the case, solutions of (2.13) must be determined on subdomains of S and related by jump conditions across their common boundaries where ∇h is discontinuous. Our solution method can easily be adapted to this situation.

We note that use of (2.12) in the boundary condition (2.6) implies that

$$\left.\begin{aligned} \phi(x, d) = \mathrm{e}^{2\mathrm{i}\beta d}\phi(x, -d), \\ \phi_y(x, d) = \mathrm{e}^{2\mathrm{i}\beta d}\phi_y(x, -d), \end{aligned}\right\} \quad -\infty < x < \infty, \tag{2.14}$$

and that (2.11) leads to

$$\phi(x, y) \sim \sum_{m=-r}^{s} \{A_m^{\pm}\mathrm{e}^{\mp\mathrm{i}\alpha_m x} + B_m^{\pm}\mathrm{e}^{\pm\mathrm{i}\alpha_m x}\}\mathrm{e}^{\mathrm{i}\beta_m y}, \quad x \to \pm\infty, \ -d \leqslant y \leqslant d. \tag{2.15}$$

The function $\phi(x, y)$, which determines the approximation to Φ, is completely

defined by (2.13), (2.14) and (2.15). The last condition is to be replaced by $\phi \to 0$ as $|x| \to \infty$ in S, in the case where $|\beta_m| > k_0$ for $m \in \mathbb{Z}$.

We note from the structure of the approximation (2.12) that it includes the far-field separation solutions $\Phi_{m,0}$ $(m = 0, 1, \ldots)$ given in (2.8), but it excludes all of the evanescent modes $\Phi_{m,n}$ for $n = 1, 2, \ldots$ associated with the vertical eigenfunctions $\cos k_n(z + h_0)$.

It is convenient at this point to transform the equation (2.13) into its canonical form, by writing

$$\phi(x, y) = \{u_0(h_0)/u_0(h(x, y))\}^{1/2}\psi(x, y). \tag{2.16}$$

Then ψ satisfies

$$\left.\begin{aligned} \nabla^2\psi + \kappa(x, y)\psi = 0, \quad (x, y) \in S, \\ \kappa(x, y) = k^2 + A\nabla^2 h + B(\nabla h)^2, \end{aligned}\right\} \tag{2.17}$$

where $A(x, y)$ and $B(x, y)$, which include the functions u_1 and u_2 of (2.13), are given by

$$A = -2k/(K + \sinh K),$$

$$B = k^2\{K^4 + 4K^3 \sinh K + 3K^2(2\cosh^2 K + 1) + 18K \sinh K + 3\sinh^2 K(2\cosh K + 5)\}/\{3(K + \sinh K)^4\},$$

the abbreviation $K = 2kh$ having been used.

The remaining conditions to be satisfied by ψ derive from (2.14) and (2.15) and are

$$\left.\begin{aligned} \psi(x, d) = e^{2i\beta d}\psi(x, -d), \\ \psi_y(x, d) = e^{2i\beta d}\psi_y(x, -d), \end{aligned}\right\} \quad -\infty < x < \infty, \tag{2.18}$$

since $u_0(h(x, d)) = u_0(h(x, -d))$, and

$$\psi(x, y) \sim \sum_{m=-r}^{s} \{A_m^{\pm} e^{\mp i\alpha_m x} + B_m^{\pm} e^{\pm i\alpha_m x}\} e^{i\beta_m y}, \quad x \to \pm\infty, \ -d \leqslant y \leqslant d, \tag{2.19}$$

if (2.10) holds, or

$$\psi(x, y) \to 0, \quad |x| \to \infty, \ -d \leqslant y \leqslant d, \tag{2.20}$$

otherwise.

We shall solve the boundary value problem for ψ in both cases by reformulating it as an integral equation, making use of the fact that, for $(x, y) \in S_0$, (2.17) reduces to the Helmholtz equation

$$\{\nabla^2 + k_0^2\}\psi = 0.$$

We therefore define the Green's function $G(x, y|\xi, \eta)$ by

$$\left.\begin{aligned} &\{\nabla^2 + k_0^2\}G = \delta(x - \xi)\delta(y - \eta), \quad (x, y) \in S, \\ &G(x, d|\xi, \eta) = e^{2i\beta d}G(x, -d|\xi, \eta), \quad -\infty < x < \infty, \\ &G_y(x, d|\xi, \eta) = e^{2i\beta d}G_y(x, -d|\xi, \eta), \quad -\infty < x < \infty, \\ &G \text{ bounded as } |x| \to \infty, \quad -d < y < d, \end{aligned}\right\} \tag{2.21}$$

where $(\xi, \eta) \in S$. It is easy to derive G by seeking its expansion in the set $e^{i\beta_m y}$ $(m \in \mathbb{Z})$,

giving

$$G(x,y|\xi,\eta) = -\frac{1}{4d}\sum_{m=-\infty}^{\infty}\frac{\mathrm{e}^{-\gamma_m|x-\xi|}\mathrm{e}^{\mathrm{i}\beta_m(y-\eta)}}{\gamma_m}, \tag{2.22}$$

where the quantities γ_m and β_m are as previously defined.

Linton (1998) has recently determined this form of G and has also derived alternative representations which are invaluable for computational purposes; one such representation is due to Ewald's summation method and is given in Linton (1998) to be

$$G(x,y|\xi,\eta) = -\frac{1}{4}\sum_{m=-\infty}^{\infty}\frac{\mathrm{e}^{\mathrm{i}\beta_m y'}}{2\gamma_m d}\left[\mathrm{e}^{\gamma_m x'}\mathrm{erfc}\left(\frac{\gamma_m d}{2\hat{a}}+\frac{\hat{a}x'}{d}\right)+\mathrm{e}^{-\gamma_m x'}\mathrm{erfc}\left(\frac{\gamma_m d}{2\hat{a}}-\frac{\hat{a}x'}{d}\right)\right]$$
$$-\frac{1}{4\pi}\sum_{m=-\infty}^{\infty}\mathrm{e}^{\mathrm{i}2\beta md}\sum_{n=0}^{\infty}\frac{1}{n!}\left(\frac{kd}{2\hat{a}}\right)^{2n}E_{n+1}\left(\frac{\hat{a}^2 r_m^2}{d^2}\right)$$

where $x' = x-\xi$, $y' = y-\eta$, $\mathrm{erfc}(x)$ is the complementary error function, $E_n(x) = \int_1^\infty \mathrm{e}^{-xt}/t^n \mathrm{d}t$ is the exponential integral and

$$r_m = x'^2 + (y'-2md)^2, \quad m \in \mathbb{Z}.$$

Note that the periodicity differs from that in Linton (1998) by a factor of two, whilst Linton's free parameter a is replaced here by $2\hat{a}$. We choose a value of $\hat{a}=1$ for our calculations, though this could no doubt be optimized. As $r_0 \to 0$ the behaviour of the Green's function is logarithmic, such that

$$\tilde{G}(x,y|\xi,\eta) = G(x,y|\xi,\eta) - \frac{1}{4\pi}E_1(\hat{a}^2 r_0^2/d^2)$$
$$\sim G(x,y|\xi,\eta) - \frac{1}{2\pi}\log(r_0/d) \quad \text{as} \quad r_0 \to 0 \tag{2.23}$$

is regular everywhere.

The main properties of G follow most easily from the form (2.22), however. We first note the asymmetry relation

$$G(x,-y|\xi,-\eta) = G(\xi,\eta|x,y), \tag{2.24}$$

which is induced by the mixed boundary conditions. Other useful identities follow in the case where (2.10) holds, for then

$$G(x,y|\xi,\eta) \sim -\frac{\mathrm{i}}{4d}\sum_{m=-r}^{s}\frac{\mathrm{e}^{\mathrm{i}\alpha_m|x-\xi|}\mathrm{e}^{\mathrm{i}\beta_m(y-\eta)}}{\alpha_m}, \quad |x-\xi|\to\infty, \ -d<y,\ \eta<d, \tag{2.25}$$

$$G(x,y|\xi,\eta) = \bar{G}(\xi,\eta|x,y) - \frac{\mathrm{i}}{2d}\sum_{m=-r}^{s}\frac{\cos(\alpha_m(x-\xi))\mathrm{e}^{\mathrm{i}\beta_m(y-\eta)}}{\alpha_m} \tag{2.26}$$

and

$$G(x,-y|\xi,-\eta) = \bar{G}(x,y|\xi,\eta) + \frac{\mathrm{i}}{2d}\sum_{m=-r}^{s}\frac{\cos(\alpha_m(x-\xi))\mathrm{e}^{-\mathrm{i}\beta_m(y-\eta)}}{\alpha_m}. \tag{2.27}$$

If (2.10) does not apply then (2.25), (2.26) and (2.27) are replaced by

$$\left.\begin{aligned} &G \to 0, \quad |x-\xi|\to\infty, \ -d<y,\ \eta<d,\\ &G(x,y|\xi,\eta) = \bar{G}(\xi,\eta|x,y). \end{aligned}\right\} \tag{2.28}$$

We note in particular that G is hermitian in this case.

We shall later make use of Green's second identity in the form

$$\lim_{X\to\infty}\iint_{S_X}\{U\nabla^2 V - V\nabla^2 U\}\,\mathrm{d}x\,\mathrm{d}y = \lim_{X\to\infty}\int_{C_X}\left\{U\frac{\partial V}{\partial n} - V\frac{\partial U}{\partial n}\right\}\mathrm{d}c, \tag{2.29}$$

where S_X denotes the domain S truncated at $x = \pm X$, and $\partial/\partial n$ is the outward normal derivative on the boundary C_X of S_X. In particular, if the identity is applied to ψ and G, it will result in an integral over the finite domain S_h, and this is the basis of our solution method.

From this point we need to separate the trapping and scattering problems and we consider them in turn in the following two sections.

3. The trapping problem

3.1. *Derivation of an integral equation*

Non-trivial solutions of the boundary value problem given by (2.17), (2.18) and (2.20), namely

$$\left.\begin{aligned}&\nabla^2\psi + \kappa(x,y)\psi = 0, \quad (x,y)\in S,\\ &\psi(x,d) = \mathrm{e}^{2\mathrm{i}\beta d}\psi(x,-d),\ \psi_y(x,d) = \mathrm{e}^{2\mathrm{i}\beta d}\psi_y(x,-d), \quad -\infty < x < \infty,\\ &\psi(x,y)\to 0, \quad |x|\to\infty,\end{aligned}\right\} \tag{3.1}$$

approximate localized waves travelling over the varying part of the topography. By analogy, we adopt the description Rayleigh–Bloch in the present context to describe such solutions and β, which plays the part of an eigenvalue parameter here, is then known as the Rayleigh–Bloch parameter. Supposing the topography to be fixed, we therefore seek values $\beta(k_0)$ for which (3.1) has a non-trivial solution, for each value of the wavenumber k_0. Equivalently, $k_0(\beta)$ can be regarded as the eigenvalue parameter and this is the more convenient viewpoint to adopt.

The following deductions can be made about the solutions of (3.1) and these inform the computational method which we shall use. With k_0 fixed, we note that (3.1) is unchanged if β is replaced by $\beta + j\pi/d$ for $j = \pm 1, \pm 2, \ldots$, from which it follows that we may restrict β to the interval $0 \leqslant \beta \leqslant \pi/d$ and use periodicity to continue the solution to other values. Further, by writing $\pi/d - \beta$ in place of β we deduce that if there is a non-trivial solution ψ of (3.1) for $k_0(\beta)$ then there is a non-trivial solution $\bar{\psi}$ for $k_0(\pi/d - \beta)$. From these observations we deduce that the eigenvalues satisfy the relationships

$$k_0(\beta) = k_0(\pi/d - \beta), \quad k_0(\beta) = k_0(\beta + j\pi/d), \quad j = \pm 1, \pm 2\ldots, \tag{3.2}$$

and that we can confine attention to the interval $0 \leqslant \beta \leqslant \pi/2d$. The trapping problem requires that $|\beta_m| > k_0$ for all $m \in \mathbb{Z}$, implying that the eigenvalues must satisfy $\beta > k_0(\beta)$ and $\pi/d - \beta > k_0(\beta)$ and, since $\pi/2d \geqslant \beta$, these requirements reduce to

$$\pi/2d \geqslant \beta > k_0(\beta) > 0. \tag{3.3}$$

In the special case when $\beta = 0$, it is also possible to seek trapped mode solutions in the interval $0 < k_0 < \pi/d$ provided that the boundary conditions in (3.1) are replaced either by $\psi(x,0) = \psi(x,d) = 0$ or by $\psi_y(x,0) = \psi_y(x,d) = 0$, for $-\infty < x < \infty$. These conditions arise only if the topography is symmetric about the planes $y = 0$ and $y = d$.

Applying (2.29) to ψ and G, noting that (2.28) applies in the trapping problem, we

easily obtain

$$\psi(x,y) = -\iint_{S_h} G(x,y|\xi,\eta)\ell(\xi,\eta)\psi(\xi,\eta)\,\mathrm{d}\xi\,\mathrm{d}\eta, \tag{3.4}$$

for all $(x,y) \in S$, where

$$\ell(x,y) = \kappa(x,y) - k_0^2. \tag{3.5}$$

The equation (3.4) serves both as an integral equation for ψ in S_h, with (x,y) restricted to S_h, and as an integral representation for ψ in $S_0 = S\backslash S_h$ which becomes effective once the integral equation has been solved.

The integral equation can be written

$$\psi = \mathsf{KL}\psi \tag{3.6}$$

where the operators K and L on $L_2(S_h)$ are defined by

$$(\mathsf{K}\psi)(x,y) = -\iint_{S_h} G(x,y|\xi,\eta)\psi(\xi,\eta)\,\mathrm{d}\xi\,\mathrm{d}\eta, \quad (\mathsf{L}\psi)(x,y) = \ell(x,y)\psi(x,y), \quad (x,y) \in S_h.$$

Both operators are self-adjoint, K because of the hermitian property of G given in (2.28) and L because ℓ is real-valued. Moreover, K is a positive operator (see the Appendix) and therefore, using the inner product

$$(p,q) = \iint_{S_h} p\,\bar{q},$$

it follows that $(\mathsf{L}\psi,\psi) = (\mathsf{K}(\mathsf{L}\psi),(\mathsf{L}\psi)) > 0$ for every non-trivial solution ψ. Thus every solution of (3.4) must be such that

$$I_h = \iint_{S_h} \ell(x,y)|\psi(x,y)|^2\,\mathrm{d}x\,\mathrm{d}y > 0, \tag{3.7}$$

and Rayleigh–Bloch waves exist only if $\ell(x,y) > 0$, at least on some subdomain of S_h.

More generally, if $\mu\psi = \mathsf{KL}\psi$ then $(\mu\psi,\mathsf{L}\psi) = (\mathsf{KL}\psi,\mathsf{L}\psi)$ and $(\mathsf{L}\psi,\mu\psi) = (\mathsf{L}\psi,\mathsf{KL}\psi)$, which together imply that $\mu(\mathsf{L}\psi,\psi) = \bar{\mu}(\mathsf{L}\psi,\psi) = (\mathsf{LKL}\psi,\psi)$. Therefore $(\mu-\bar{\mu})(\mathsf{L}\psi,\psi) = 0$ from which it follows that the eigenvalues of KL are all real, since $(\mathsf{L}\psi,\psi) \neq 0$ follows from the positivity of K.

The condition (3.7) can be readily interpreted if we assume that $h(x,y)$ is a slowly varying function, for then

$$\ell = k^2 - k_0^2 + O(\epsilon)$$

follows from (2.17) and (3.5), ϵ denoting a small parameter. Since k is a decreasing function of h, we infer that for Rayleigh–Bloch waves to be possible, at least some of the varying topography must be elevated above the level $h = h_0$. A depression below this level can occur, provided that it is compensated by an elevation sufficient to ensure that the condition (3.7) is satisfied.

Against this background we now locate the non-trivial solutions of (3.4) numerically.

3.2. *Discretization of the integral equation*

We assume for simplicity that S_h coincides with the rectangle $S_{ab} = [-a,a] \times [-b,b]$, where $b \leqslant d$. Let us define the points

$$\frac{x_i}{a} = \frac{(2i-1)}{N_x} - 1, \quad i = 1,\ldots,N_x, \qquad \frac{y_i}{b} = \frac{(2i-1)}{N_y} - 1, \quad i = 1,\ldots,N_y,$$

and, in the interest of compactness of notation, we introduce the vectors

$$\boldsymbol{x}_{i+(j-1)N_x} = (x_i, y_j), \quad i = 1, \ldots, N_x, \;\; j = 1, \ldots N_y, \tag{3.8}$$

representing a rectangular array of points on S_{ab}. The double integral in equation (3.4) is approximated simply by application of the rectangle midpoint rule and evaluating the integral at the points $(\xi, \eta) = \boldsymbol{x}_i$, $i = 1, \ldots, N_x N_y$. Thus, for $(x, y) \neq \boldsymbol{x}_j$, $j = 1, \ldots, N_x N_y$, we obtain

$$(\mathsf{KL}\psi)(x, y) \approx -\frac{4ab}{N_x N_y} \sum_{i=1}^{N_x N_y} G(x, y|\boldsymbol{x}_i)\ell(\boldsymbol{x}_i)\psi(\boldsymbol{x}_i). \tag{3.9}$$

Since G has a logarithmic singularity, we write $G(x, y|\xi, \eta) = \tilde{G}(x, y|\xi, \eta) + \log(r_0/d)/(2\pi)$ as $r_0 = \{(x-\xi)^2 + (y-\eta)^2\}^{1/2} \to 0$ where $\tilde{G}$ is regular and defined in (2.23). Then, for $(x, y) = \boldsymbol{x}_j$,

$$(\mathsf{KL}\psi)(\boldsymbol{x}_j) \approx -\frac{4ab}{N_x N_y} \left[\sum_{\substack{i=1 \\ \neq j}}^{N_x N_y} G(\boldsymbol{x}_j|\boldsymbol{x}_i)\ell(\boldsymbol{x}_i)\psi(\boldsymbol{x}_i) - \tilde{G}(\boldsymbol{x}_j|\boldsymbol{x}_j)\ell(\boldsymbol{x}_j)\psi(\boldsymbol{x}_j) \right] + S_j,$$

where

$$S_j = \frac{1}{4\pi} \int_{-X}^{X} \int_{-Y}^{Y} \log\left[\frac{\xi^2 + \eta^2}{d^2}\right] \ell(\boldsymbol{x}_j + (\xi, \eta))\psi(\boldsymbol{x}_j + (\xi, \eta)) \mathrm{d}\xi \mathrm{d}\eta$$

with $X = a/N_x$, $Y = b/N_y$, is the contribution to the integral from the logarithm in the rectangle of sides $2X$ and $2Y$ having $\boldsymbol{x}_j$ at its centre. In accordance with the use of the rectangle midpoint rule, ℓ and ψ are evaluated at the centre of the rectangle, $\xi = \eta = 0$. Thus

$$S_j \approx \frac{4ad}{N_x N_y} \ell(\boldsymbol{x}_j)\psi(\boldsymbol{x}_j) R_j$$

where

$$\begin{aligned} R_j &= \frac{1}{16\pi XY} \int_{-X}^{X} \int_{-Y}^{Y} \log \frac{\xi^2 + \eta^2}{d^2} \mathrm{d}\xi \mathrm{d}\eta \\ &= \frac{1}{4\pi} \left[\log\left(\frac{X^2 + Y^2}{d^2}\right) - 3 + \frac{Y}{X} \tan^{-1}\left(\frac{X}{Y}\right) + \frac{X}{Y} \tan^{-1}\left(\frac{Y}{X}\right) \right]. \end{aligned}$$

The discretization described here is valid only for rectangular S_h. For non-rectangular S_h, an appropriate alternative discretization should be implemented. For the purposes of this paper, it is sufficient to continue with topography defined on a rectangular domain.

Using (3.9) in (3.4) and evaluating at $(x, y) = \boldsymbol{x}_j$, $j = 1, \ldots, N_x N_y$, results in the discrete system

$$-\frac{4ab}{N_x N_y} \sum_{i=1}^{N_x N_y} G_{ij}\ell(\boldsymbol{x}_i)\psi(\boldsymbol{x}_i) = \psi(\boldsymbol{x}_j), \quad j = 1, \ldots, N_x N_y, \tag{3.10}$$

where

$$G_{ij} = \begin{cases} G(\boldsymbol{x}_j|\boldsymbol{x}_i), & i \neq j, \\ \tilde{G}(\boldsymbol{x}_j|\boldsymbol{x}_j) + R_j, & i = j, \end{cases} \tag{3.11}$$

and $G_{ij} = \bar{G}_{ji}$ as a direct consequence of (2.28). If the topography is symmetric about the planes $x = 0$ or $y = 0$, or both, advantage may be taken of the various 'symmetry' relationships for G outlined towards the end of § 2 to improve the numerical efficiency. Details of the system resulting from symmetric geometries are rather laborious, and the reader is referred to Porter & Evans (1999) where a similar procedure was implemented.

3.3. *Numerical method and results*

Numerical approximations to Rayleigh–Bloch solutions are given by values of $k_0(\beta)$ corresponding to non-trivial solutions of (3.10). These may be computed numerically in one of two ways. One method is to locate, as a function of k_0, those (real) eigenvalues equal to unity of the matrix having elements

$$-\frac{4ab}{N_x N_y} G_{ij} \ell(\boldsymbol{x}_i). \tag{3.12}$$

This approach has the advantage that standard library routines for computing eigenvalues of matrices also provide the corresponding eigenvectors. For those eigenvalues equal to unity, the corresponding eigenvectors will have as elements the values of ψ at $(x, y) = \boldsymbol{x}_i$, $i = 1, \ldots, N_x N_y$ (scaled by an arbitrary constant). These may be used in conjunction with (3.9) in (3.4) to evaluate $\psi(x, y)$ for any $(x, y) \in S$. This method is used later to produce free surface elevations.

A more computationally efficient method is to seek, as a function of k_0, the zeros of the determinant of the matrix in (3.10) having elements

$$\frac{4ab}{N_x N_y} G_{ij} \ell(\boldsymbol{x}_i) + \delta_{ij},$$

which is real since the eigenvalues are real, a result which was established earlier in § 3.1.

There is, of course, a huge number of bed geometries that we could investigate for Rayleigh–Bloch solutions. The only restrictions that have been placed on the topography in the development of our formulation of the problem is that it be smooth everywhere in S_h, that it should join the constant depth h_0 smoothly and, on account of the numerical discretization used, that the periodic arrays must have elements which vary on a rectangular patch, S_{ab}. We consider three generic periodic topographies which will allow us to assess the influence of certain topographical features and from which we can confidently infer some general conclusions.

First, consider the bed elevation given by

$$h(x, y)/h_0 = \begin{cases} 1 - \frac{1}{4}A_+(1 + \cos(\pi x/a))(1 + \cos(\pi y/b)), & |x| \leqslant a,\ |y| \leqslant b \leqslant d, \\ 1, \quad \text{elsewhere}, \end{cases} \tag{3.13}$$

which has cosine variations in both x and y, joins the depth h_0 smoothly at $|x| = a$, $|y| \leqslant b$ and $|y| = b$, $|x| \leqslant a$ and allows for a flat region of depth h_0 in $b \leqslant |y| \leqslant d$. The bed has no depression below h_0 and the maximum bed elevation, non-dimensionalized with respect to h_0, is A_+ and occurs at $x = y = 0$.

It turns out, numerically, that at least one Rayleigh–Bloch solution exists for every geometrical configuration given by (3.13) and for every value of β in $0 < \beta \leqslant \pi/2d$.

Table 1 shows the convergence of the numerical scheme with N_x and N_y for some typical geometrical parameters using $h(x, y)$ defined by (3.13). The value of $\beta = \pi/2d$

$N_x \times N_y$	$A_+/h_0 = \frac{1}{4}$	$A_+/h_0 = \frac{1}{2}$	$A_+/h_0 = \frac{3}{4}$
4×4	1.56708	1.55284	1.51915
6×6	1.56702	1.55171	1.51372
8×8	1.56702	1.55167	1.51313
10×10	1.56702	1.55167	1.51302
12×12	1.56702	1.55166	1.51299

TABLE 1. Convergence of $k_0 d$ with grid sizes N_x, N_y for maximum amplitudes $A_+/h_0 = \frac{1}{4}, \frac{1}{2}, \frac{3}{4}$ for the bed elevation defined by (3.13) with $d/h_0 = 1$, $b/d = 1$, $a/d = 1$ and $\beta d = \pi/2$.

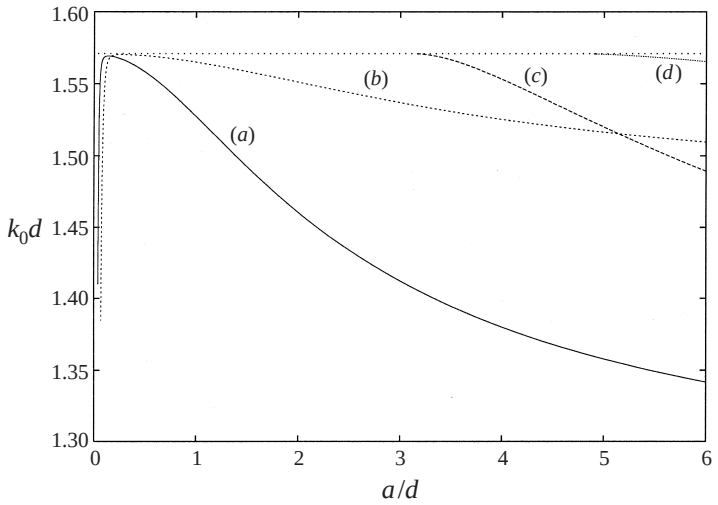

FIGURE 1. The variation of trapped mode wavenumber $k_0 d$ with length of bed a/d for bed elevation (3.13) having, $b/d = 1$, $d/h_0 = 2$, $A_+ = \frac{1}{2}$ and $\beta d = \pi/2$.

is chosen since it is at this value that there is the largest difference between k_0 and β; away from $\beta = \pi/2d$, Rayleigh–Bloch solutions tend rapidly to $k_0/\beta = 1$. It can be seen that the accuracy of the method, even for a 'steep' topography ($A_+/h_0 = \frac{3}{4}$), is remarkably good, with a 10×10 grid size sufficient to claim four decimal places in all cases. All results produced in the figures that follow use values of $N_x = [16a/d]$, $N_y = 16$ where $[x]$ is the integer part of x.

Before giving results for general β, it proves instructive to examine the special case of $\beta d = \pi/2$.

In figure 1 curves are plotted showing the variation of the dimensionless trapped mode wavenumber $k_0 d$ with aspect ratio, a/d, of the varying part of the topography for the symmetric geometry defined by (3.13) with $b/d = 1$, $d/h_0 = 2$, $A_+ = \frac{1}{2}$ and for $\beta d = \pi/2$. As $a/d \to 0$, the topography steepens and numerical accuracy is lost as demonstrated in the curves labelled (a) and (b). The correct behaviour of trapped modes in the limit $a/d \to 0$ is $k_0 d \to \pi/2$ and larger values of N_x, N_y can be taken to resolve this case numerically. The curves labelled (a) and (b) in figure 1 correspond, for $\beta d = \pi/2$, to the trapped modes in a strip of width $2d$ having Neumann and Dirichlet boundary conditions, respectively, on the walls $y = \pm d$. In the former case, this motion corresponds to the trapped modes in a hard-walled channel of width $2d$. It is also expected, by analogy with many other trapped mode problems in waveguides,

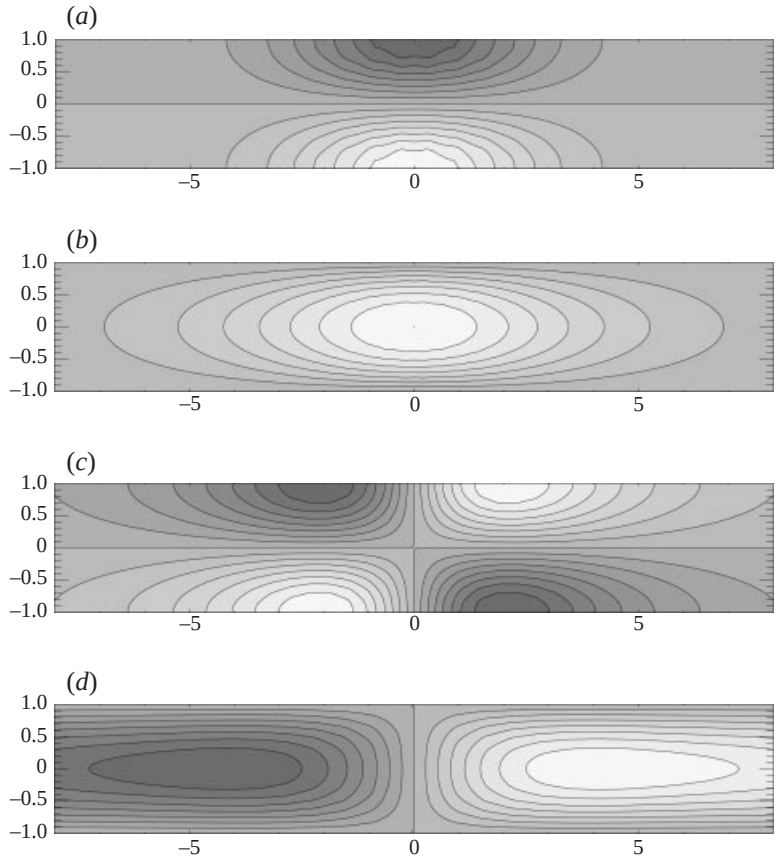

FIGURE 2. A snapshot of the free surface for the trapped modes present for the bed elevation (3.13) with $a/d = 5$, $b/d = 1$, $d/h_0 = 2$, $A_+ = \frac{1}{2}$ and $\beta d = \pi/2$; (*a–d*) correspond to the curves in figure 1.

that increasing the length, a, of the trapping structure with d fixed will result in further modes and this is indeed observed to be the case. Since the topography is symmetric about the plane $x = 0$ coinciding with the infinite periodic array, trapped mode solutions must either be symmetric or antisymmetric about this plane. Thus curves (*a*) and (*b*) represent wave motions symmetric about $x = 0$, whilst as the strip of topography becomes broader, further modes labelled (*c*) and (*d*) appear through the cut-off wavenumber $k_0 d = \pi/2$ and correspond to wave motions which are antisymmetric about the plane $x = 0$ and have Neumann and Dirichlet conditions (respectively) on the walls ($y = \pm d$). The various symmetries of the trapped modes described above are more clearly illustrated in figure 2 where a value of $a/d = 5$ has been chosen and where axes are non-dimensionalized by d. It can be seen that in addition to the Neumann conditions in (*a*) and (*c*) and Dirichlet conditions in (*b*) and (*d*) on the walls $y/d = \pm 1$, the modes also satisfy Dirichlet and Neumann conditions respectively on the centreline, $y = 0$, of the guide.

The presence of the trapped mode labelled (*b*) in figures 1 and 2 satisfying Dirichlet conditions on $y/d = \pm 1$ and a Neumann condition on $y = 0$ is somewhat unexpected. This is because if, instead of varying periodic topography, an infinite periodic array of symmetric vertical cylinders were considered, the existence of a trapped mode solution satisfying Dirichlet conditions on $y = \pm d$ and a Neumann condition on

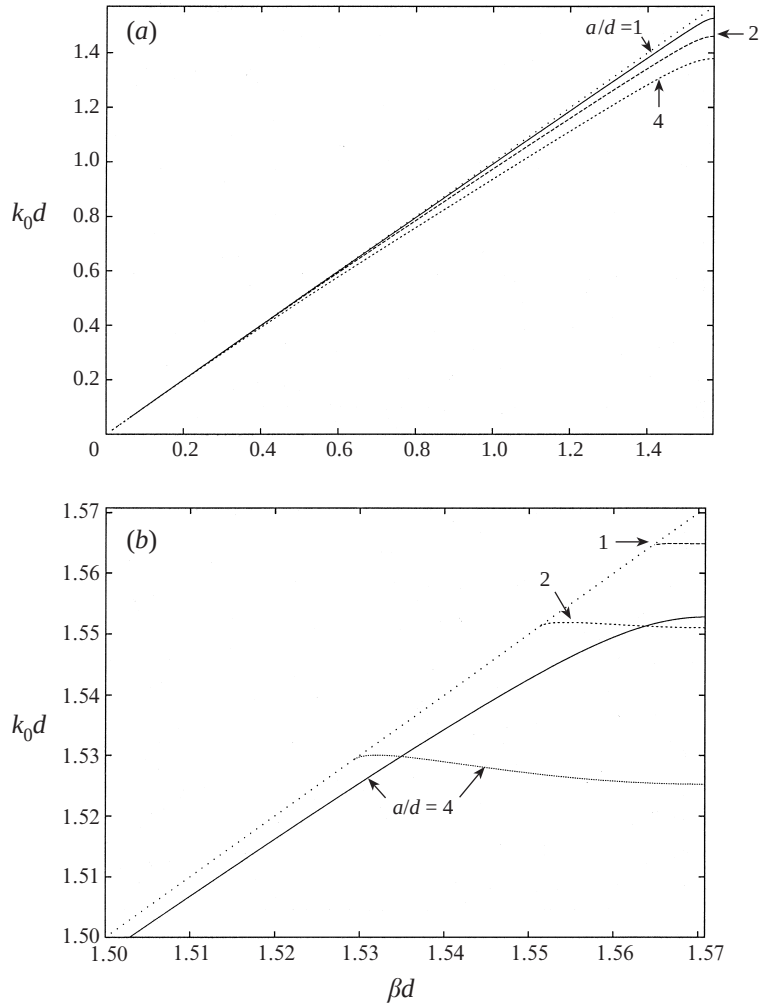

FIGURE 3. Curves of k_0d against βd for geometry (3.13) with $d/h_0 = 2$, $b/d = 1$, $A_+/h_0 = \frac{1}{2}$, $a/d = 1, 2, 4$ (shown against curves). The cut-off $k_0 = \beta$ is denoted by $(\cdots)$. (b) An enlargement of the top right-hand corner of (a) showing additional modes (dashed curves) associated with symmetric Dirichlet trapped modes (solid curve) associated with antisymmetric Neumann trapped mode.

$y = 0$ would be ruled out by a proof of McIver & Linton (1995). This feature will be discussed further in § 3.4.

In figure 3(a, b) we show how the non-dimensional trapped mode wavenumbers, k_0d, vary with Rayleigh–Bloch parameter βd. We have chosen $d/h_0 = 2$, $b/d = 1$ and $A_+/h_0 = \frac{1}{2}$ and present curves for values of $a/d = 1, 2, 4$. It can be seen from figure 3(a) that there exists at least one Rayleigh–Bloch trapped wave for $0 < \beta d \leqslant \pi/2$ for every value of a/d chosen, and for any given value of βd, the value of k_0d is reduced as a/d increases. In addition, there exist further modes for βd close enough to $\pi/2$, shown separately in the enlarged figure 3(b), which quickly disappear through the cut-off as βd is reduced from $\pi/2$. When $\beta d = \pi/2$, the trapped mode wavenumbers for the different values of a/d may be read from figure 1, and the type of mode can be ascertained from the discussion surrounding figures 1 and 2. The behaviour

of these additional modes is very interesting. To the authors' knowledge all previous results for Rayleigh–Bloch wavenumbers $k_0(\beta)$ have been monotonic increasing with increasing β in $0 < \beta d \leqslant \pi/2$ (as clearly demonstrated in figure 3*a*). However, three of the curves shown in figure 3(*b*) corresponding to the three values of $a/d = 1, 2, 4$ show quite different behaviour. This may be explained by the fact that each of the curves exhibiting this behaviour is connected with the existence of a trapped mode for $\beta d = \pi/2$ which corresponds to a *symmetric Dirichlet trapped mode* in a parallel channel containing symmetric topography and this type of mode is known to not exist in cases of infinite periodic arrays of vertical cylinders (see later). The one additional Rayleigh–Bloch solution shown in 3(*b*) which does not possess this unusual behaviour exists for $a/d = 4$ only and disappears through the cut-off at a value of $\beta d \approx 1.42$. This solution corresponds to the trapped mode labelled (*c*) in figure 1; that is, a Neumann mode but with antisymmetry about the line $x = 0$ (see figure 2*c*).

When $\beta = 0$ trapped modes are also present, though these are not illustrated in the figures. These trapped modes satisfy Dirichlet conditions on the planes $x = 0$ and $x = d$ and occur at wavenumbers $0 < k_0 < \pi/d$.

In Porter & Evans (1999) it was shown how trapped modes in parallel-walled waveguides having Neumann and Dirichlet conditions on the walls spanned by an arbitrary number of identical periodically spaced vertical cylinders each having symmetry about a plane perpendicular to the array could be reconstructed from Rayleigh–Bloch wave solutions for one such cylinder corresponding to certain special choices of β. The same is true when one considers periodically varying topography as is the case here. A detailed description of this process is given in § 4 of Porter & Evans (1999); because of the similarities in the governing equations only a brief summary of the main results is presented here. Thus, for M periods of topography, each symmetric about a plane perpendicular to the array, spanning a channel having Neumann conditions on the walls, the corresponding trapped mode wavenumbers are given by the solutions $k_0(\beta)$ for $\beta d = n\pi/2M$, $n = 1, \ldots, M$ (see Porter & Evans 1999). When $\beta d = \pi/2$, one must choose the solution k_0 which corresponds to a Neumann trapped mode about a single period of topography in a channel.

This connection between trapped modes about multiple periodic structures and Rayleigh–Bloch solutions for certain values of β has been confirmed by comparing the relevant solutions of the Rayleigh–Bloch problem for just one period of symmetric topography with the waveguide trapped modes for $\beta d = \pi/2$ spanned by M periods of the same symmetric topography using the bed elevation

$$h(x, y)/h_0 = \begin{cases} 1 - \frac{1}{4}A_+(1 + \cos(\pi x/a))(1 + \cos(\pi M y/d)), & |x| \leqslant a,\ |y| \leqslant d, \\ 1, \quad \text{elsewhere.} \end{cases}$$

The second geometry that we consider is defined by the bed elevation

$$h(x, y)/h_0 = \begin{cases} 1 - \frac{1}{4}(1 + \cos(\pi x/a))[(A_+ + A_-) + (A_+ - A_-)\cos(\pi y/d)], & \begin{matrix} |x| \leqslant a, \\ |y| \leqslant d, \end{matrix} \\ 1, \quad \text{elsewhere,} \end{cases} \tag{3.14}$$

which again has cosine profiles in both x and y but which allows both elevations and depressions to non-dimensional depths A_+ and A_- respectively.

As outlined at the end of § 3.1, it would seem likely that Rayleigh–Bloch waves can be supported above periodic topography with depression below the constant depth h_0 provided the depression is offset by a large enough elevated topography to ensure that the implicit condition (3.7) is satisfied, and this turns out to be the case. In figure 4 we

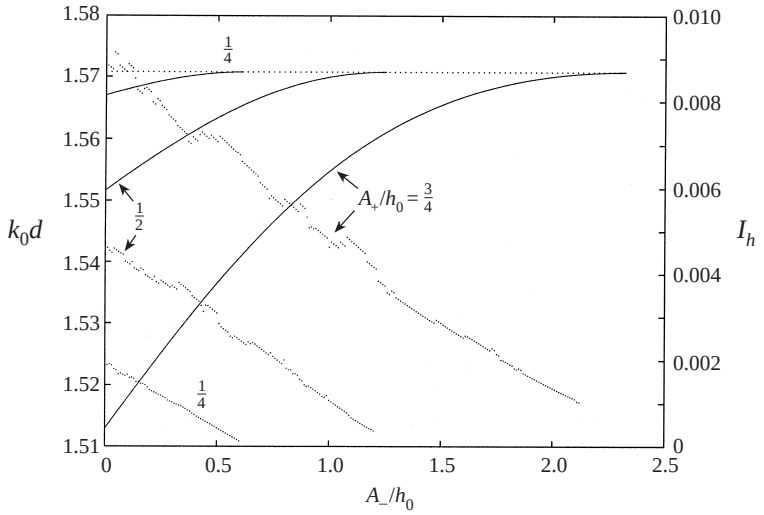

FIGURE 4. Variation of trapped mode wavenumber (solid curves, left-hand scale) and I_h (dots, right-hand scale) with depression A_-/h_0 for the bed elevation (3.13) with $d/h_0 = 1$, $a/d = 1$, $\beta d = \pi/2$ and elevations $A_+/h_0 = \frac{1}{4}, \frac{1}{2}, \frac{3}{4}$ (shown against curves).

show curves of trapped mode wavenumber k_0d (solid curves on the left-hand scale) against depression A_-/h_0 for the geometry (3.14) where $d/h_0 = 1$, $a/d = 1$. The three curves correspond to maximum elevations of $A_+/h_0 = \frac{1}{4}, \frac{1}{2}, \frac{3}{4}$, and corresponding to each solid curve is a dotted curve which records the value of I_h defined by (3.7) (on the right-hand scale) as A_-/h_0 varies. The evaluation of I_h is not accurate, for steep topographies in particular, on account of the simple approximation to the integral and the relatively coarse numerical gridding of S_h. From (3.7) the condition for a Rayleigh–Bloch wave to exist is $I_h > 0$, and this is certainly confirmed in figure 4. Indeed, it would appear that the condition $I_h > 0$ represents a fairly tight bound on the existence of Rayleigh–Bloch waves when there is both elevation and depression in the topography.

The third and final topography discussed in this section is defined by the depth function

$$h/h_0 = \begin{cases} 1 - \frac{1}{4}A_+(1 + \cos(\pi x/a))[1 + \frac{4}{9}\sqrt{3}(\cos(\pi y/d) + \frac{1}{2}\sin(2\pi y/d))], & \begin{matrix}|x| \leqslant a,\\ |y| \leqslant d,\end{matrix} \\ 1, \quad \text{elsewhere}, \end{cases} \tag{3.15}$$

which incorporates the cosine-type envelope in the x-direction used in the previous geometries, but whose cross-section in y across an element is now unsymmetric (see insert in figure 5), consisting of no depression below h_0 and with elevation to a maximum height A_+ above h_0.

The lack of symmetry in the topography does not preclude the possibility of the existence of Rayleigh–Bloch waves since it has been shown that the integral operator has real eigenvalues independently of the function $h(x, y)$. This was not the case for Rayleigh–Bloch waves in the presence of an infinite periodic array of vertical cylinders as considered by Porter & Evans (1999), when realness of a determinant, whose vanishing determined a Rayleigh–Bloch solution, could only be shown for cylinders that possessed a plane of symmetry perpendicular to the array. Thus, Porter & Evans (1999) did not seek solutions about unsymmetric cylinders for general values

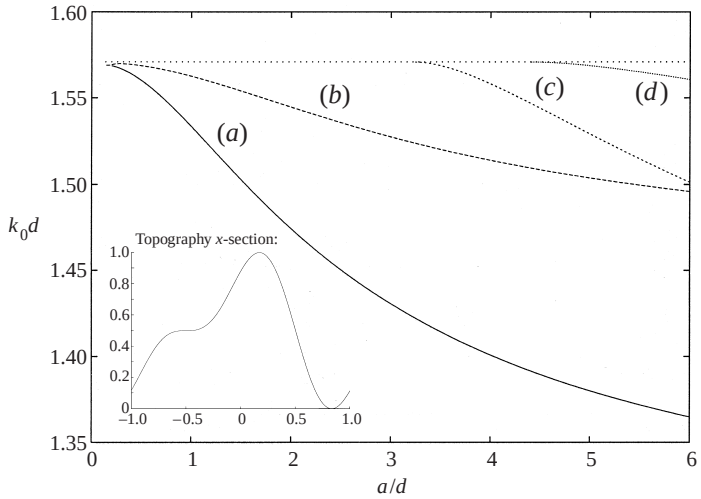

FIGURE 5. The variation of trapped mode wavenumber k_0d with length of bed a/d for the bed elevation (3.15) having $d/h_0 = 2$, $A_+ = \frac{1}{2}$ and $\beta d = \pi/2$. Insert shows section $x = 0$, $-d < y < d$ through topography.

of β since the complex nature of the determinant rendered the possibility of finding real roots unlikely. However, in the light of the results obtained in the present work, one of the authors (R. Porter) has recomputed the Rayleigh–Bloch problem for an infinite array of vertical cylinders with unsymmetric cross-section for general β, and found numerically that there do indeed appear to be zeros of a complex determinant for real values of wavenumber k_0 which correspond to Rayleigh–Bloch waves.

In figure 5 are plotted curves of Rayleigh–Bloch solutions k_0d against the width of the array, a/d, with the same parameters used for generating figure 1 but with the depth function now replaced by (3.15), having an unsymmetric cross-section as shown in the insert. Nevertheless, there exists a set of modes corresponding to those for the symmetric depth function (3.13).

3.4. *Non-existence of trapped modes*

In the previous section we showed numerically that there exists, for a value $\beta d = \pi/2$, a trapped mode with $k_0 < \beta$ for the infinite periodic array which is equivalent to a symmetric trapped mode in a channel containing elevated topography symmetric about the centreplane of the channel, with Dirichlet conditions on the walls. The existence of such a type of mode may at first seem surprising given that McIver & Linton (1995) have proved that such a trapped mode does not exist for $k_0 < \beta$ when, instead of varying topography, a uniform vertical cylinder having either Neumann or Dirichlet surface conditions is placed in the Dirichlet-walled channel.

A reworking McIver & Linton's (1995) analysis in this case is trivial, the difference being the replacement of the constant k^2 (equivalent to our k_0^2 here) with $\kappa(x, y)$, and results in an equation which is the analogue of McIver & Linton's (1995) equation (2.10), namely

$$\int_S \left(w^2(\nabla v)^2 - \frac{\phi^2}{w}(\nabla^2 w + \kappa(x,y)w) \right) \mathrm{d}x\,\mathrm{d}y = \int_{y=\pm d} \left(\phi \frac{\partial \phi}{\partial n} - \frac{\phi^2}{w}\frac{\partial w}{\partial n} \right) \mathrm{d}x, \qquad (3.16)$$

where $\phi = v/w$ and $v(x, y)$, $w(x, y)$ are both real functions (since ϕ can be taken to be real without loss of generality in this case, where ϕ satisfies real boundary

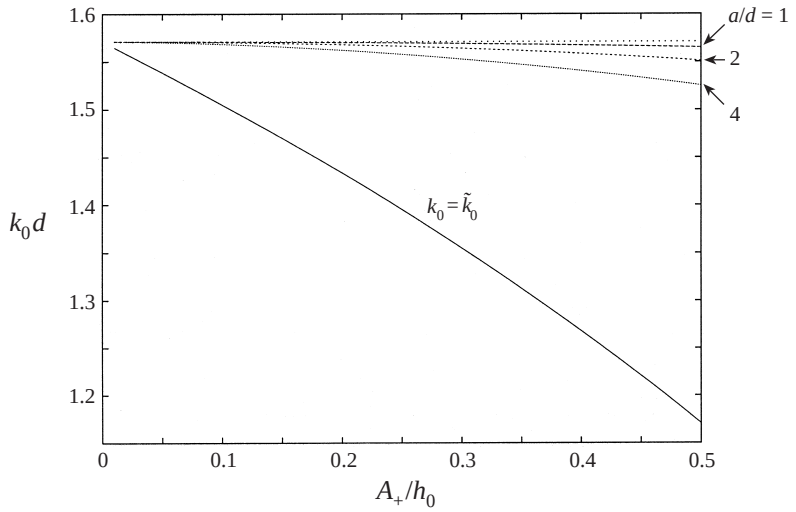

FIGURE 6. Curves of trapped mode ($\beta d = \pi/2$) frequency versus A_+/h_0 for the bed elevation (3.13) with $d/h_0 = 2$ $b/d = 1$, and for $a/d = 1, 2, 4$. The solid curve is the bounding curve $k_0 = \tilde{k}_0$ below which trapped modes are prohibited by the non-existence proof of § 3.4.

conditions) and w is positive in the strip S. As in McIver & Linton (1995) we choose $w(x, y) = \cos \alpha y$ which forces $\alpha < \pi/2d$. The right-hand side of (3.16) vanishes owing to the Dirichlet conditions on the walls of the channel and substituting w into (3.16), the left-hand side is seen to be positive if $\kappa_{max} \equiv \max_{(x,y)\in S}\{\kappa(x, y)\} \leqslant \alpha < \pi/2d$ from which it then follows that $\phi \equiv 0$. Thus the condition for the non-existence of a trapped mode in the case of varying topography in a channel having Dirichlet conditions on the walls of the channel is

$$[\kappa_{max}(k_0)]^{1/2} d < \pi/2.$$

Contrary to the case of the vertical cylinder in the channel, there now exists an interval $\tilde{k}_0 < k_0 < \pi/2d$, with $[\kappa_{max}(\tilde{k}_0)]^{1/2} = \pi/2d$, in which trapped modes may exist in the case of varying topography contained in a channel having Dirichlet wall conditions.

Results showing the bounding curve $\tilde{k}_0 d$ in a typical case are presented in figure 6 for the geometry defined by (3.13) with $d/h_0 = 2$, $b/d = 1$ as A_+/h_0 varies between 0 and $\frac{1}{2}$. From the non-existence proof above, symmetric Dirichlet trapped modes cannot exist below this curve. Also shown in figure 6 are curves of the actual symmetric Dirichlet trapped modes in this example for three different values of a/d, which are clearly contained within the allowed range for trapped modes. It is not clear from figure 6 and other results that have been computed whether the bounding curve represents a tight bound between existence and non-existence of symmetric Dirichlet trapped modes.

An extension of the methods of McIver & Linton (1995) to arbitrary β for which ϕ becomes complex-valued does not appear to yield any useful results.

4. The scattering problem

4.1. *Scattering matrix formulation*

The preliminary discussion of the scattering case in § 2 allows for $M = r + s + 1$ travelling wave modes as $|x| \to \infty$, where r and s are defined by (2.10). The most general scattering problem thus consists of linear combinations of these M modes

incident on the region of varying topography from both $x = -\infty$ and $x = +\infty$. We determine the solution of this problem by calculating the scattering properties for each individual incident mode and using superposition.

Suppose that there is a single incident wave, given by the reduced potential

$$\Phi_0(x, y, z) = \frac{\cosh\{k_0(z + h_0)\}}{\cosh(k_0 h_0)} \exp(\mathrm{i}k_0 x \cos\theta_0 + \mathrm{i}k_0 y \sin\theta_0),$$

where k_0 and the incident angle $\theta_0 \in (-\pi/2, \pi/2)$ are given. We may therefore write $\alpha_0 = k_0 \cos\theta_0$ and $\beta_0 = k_0 \sin\theta_0$ to align the notation with that used in (2.10). Assuming that d is also known, (2.7) then determines β_m for $m \in \mathbb{Z}$. The values $m = -r, \ldots, s$ for which $-k_0 < \beta_m < k_0$ can therefore be found and since $\alpha_m > 0$ the equations

$$\alpha_m = k_0 \cos\theta_m, \quad \beta_m = k_0 \sin\theta_m, \quad m = -r, \ldots, s, \tag{4.1}$$

complete the set of uniquely defined angles $\theta_m \in (-\pi/2, \pi/2)$. The dependence of this calculation on the parameter $k_0 d$ can be made explicit by using (2.7) and (4.1) to give

$$k_0 d \sin\theta_m = k_0 d \sin\theta_0 + m\pi,$$

which determines θ_m and shows that

$$r = [k_0 d(1 + \sin\theta_0)/\pi], \quad s = [k_0 d(1 - \sin\theta_0)/\pi],$$

where $[x]$ denotes the integer part of x. More generally, if k_0, d and any one of the angles θ_m are assigned, the remaining $M - 1$ angles and the values of r and s are uniquely determined.

The full set of $2M$ incident waves modes is thus

$$\Phi_m^{\pm}(x, y, z) = \frac{\cosh\{k_0(z + h_0)\}}{\cosh(k_0 h_0)} \exp(\pm\mathrm{i}k_0 x \cos\theta_m + \mathrm{i}k_0 y \sin\theta_m),$$

for $m = -r, \ldots, s$, in which k_0, d and one of the incident angles θ_m are prescribed. The scattered wave field as $x \to \pm\infty$ will in general consist of all of the modes $\Phi_m^{\pm}$, for every incident wave.

The function $\psi(x, y)$ which determines the modified mild-slope approximation to the general scattering problem is defined by (2.17), (2.18) and (2.19), where α_m and β_m are given by (4.1).

We now define the set of $2M$ component scattering problems by introducing functions $\psi_n^{\pm}(x, y)$ for $(x, y) \in S$ and $n = -r, \ldots, s$, which satisfy

$$\nabla^2 \psi_n^{\pm} + \kappa(x, y)\psi_n^{\pm} = 0, \quad (x, y) \in S, \tag{4.2}$$

$$\left.\begin{aligned} \psi_n^{\pm}(x, d) &= \mathrm{e}^{2\mathrm{i}\beta d}\psi_n^{\pm}(x, -d), \\ \psi_{ny}^{\pm}(x, d) &= \mathrm{e}^{2\mathrm{i}\beta d}\psi_{ny}^{\pm}(x, -d), \end{aligned}\right\} \quad -\infty < x < \infty, \tag{4.3}$$

and

$$\psi_n^{-}(x, y) \sim \begin{cases} \mathrm{e}^{\mathrm{i}\alpha_n x + \mathrm{i}\beta_n y} + \displaystyle\sum_{m=-r}^{s} R_{m,n}^{-} \mathrm{e}^{-\mathrm{i}\alpha_m x + \mathrm{i}\beta_m y}, & x \to -\infty, \\ \displaystyle\sum_{m=-r}^{s} T_{m,n}^{-} \mathrm{e}^{\mathrm{i}\alpha_m x + \mathrm{i}\beta_m y}, & x \to \infty, \end{cases} \tag{4.4}$$

$$\psi_n^+(x,y) \sim \begin{cases} \displaystyle\sum_{n=-r}^{s} T_{m,n}^+ \mathrm{e}^{-\mathrm{i}\alpha_m x + \mathrm{i}\beta_m y}, & x \to -\infty, \\ \mathrm{e}^{-\mathrm{i}\alpha_n x + \mathrm{i}\beta_n y} + \displaystyle\sum_{m=-r}^{s} R_{m,n}^+ \mathrm{e}^{\mathrm{i}\alpha_m x + \mathrm{i}\beta_m y}, & x \to \infty. \end{cases} \tag{4.5}$$

Clearly, the far-field conditions (2.19) are satisfied by setting

$$\psi(x,y) = \sum_{m=-r}^{s} \{A_n^- \psi_n^-(x,y) + A_n^+ \psi_n^+(x,y)\}$$

and it follows using (4.4) and (4.5) that the incoming and outgoing wave amplitudes in (2.19) are related by

$$\left.\begin{aligned} B_m^- &= \sum_{n=-r}^{s} A_n^- R_{m,n}^- + \sum_{n=-r}^{s} A_n^+ T_{m,n}^+, \\ B_m^+ &= \sum_{n=-r}^{s} A_n^- T_{m,n}^- + \sum_{n=-r}^{s} A_n^+ R_{m,n}^+, \end{aligned}\right\} \quad m = -r, \ldots, s. \tag{4.6}$$

Introducing the $M \times M$ matrices $\boldsymbol{R}_\pm = \{R_{m,n}^\pm\}$, $\boldsymbol{T}_\pm = \{T_{m,n}^\pm\}$ and the $M \times 1$ vectors $\boldsymbol{A}^\pm = \{A_m^\pm\}$, $\boldsymbol{B}^\pm = \{B_m^\pm\}$ we can write (4.6) in the concise block matrix form

$$\begin{pmatrix} \boldsymbol{B}^- \\ \boldsymbol{B}^+ \end{pmatrix} = \mathscr{S} \begin{pmatrix} \boldsymbol{A}^- \\ \boldsymbol{A}^+ \end{pmatrix}, \quad \mathscr{S} = \begin{pmatrix} \boldsymbol{R}_- & \boldsymbol{T}_+ \\ \boldsymbol{T}_- & \boldsymbol{R}_+ \end{pmatrix}, \tag{4.7}$$

where $\mathscr{S}$ is a $2M \times 2M$ scattering matrix. Instead of expressing the scattered waves in terms of the incident waves through $\mathscr{S}$, we may alternatively relate the far wavefield on the left to that on the right through a transfer matrix $\mathscr{P}$ defined by

$$\begin{pmatrix} \boldsymbol{A}^- \\ \boldsymbol{B}^- \end{pmatrix} = \mathscr{P} \begin{pmatrix} \boldsymbol{B}^+ \\ \boldsymbol{A}^+ \end{pmatrix}. \tag{4.8}$$

It follows from (4.7) that

$$\mathscr{P} = \begin{pmatrix} \boldsymbol{T}_-^{-1} & -\boldsymbol{T}_-^{-1}\boldsymbol{R}_+ \\ \boldsymbol{R}_-\boldsymbol{T}_-^{-1} & \boldsymbol{T}_+ - \boldsymbol{R}_-\boldsymbol{T}_-^{-1}\boldsymbol{R}_+ \end{pmatrix}, \quad \mathscr{P}^{-1} = \begin{pmatrix} \boldsymbol{T}_- - \boldsymbol{R}_+\boldsymbol{T}_+^{-1}\boldsymbol{R}_- & \boldsymbol{R}_+\boldsymbol{T}_+^{-1} \\ -\boldsymbol{T}_+^{-1}\boldsymbol{R}_- & \boldsymbol{T}_+^{-1} \end{pmatrix}. \tag{4.9}$$

Relationships between the components of $\mathscr{S}$ can be obtained by applying (2.29) in the four cases $(U,V) = (\psi_n^-, \bar{\psi}_p^-)$, $(\psi_n^-, \bar{\psi}_p^+)$, $(\psi_n^+, \bar{\psi}_p^-)$ and $(\psi_n^+, \bar{\psi}_p^+)$, to give

$$\left.\begin{aligned} \sum_{m=-r}^{s} \alpha_m \{R_{m,n}^- \bar{R}_{m,p}^- + T_{m,n}^- \bar{T}_{m,p}^-\} &= \sum_{m=-r}^{s} \alpha_m \{R_{m,n}^+ \bar{R}_{m,p}^+ + T_{m,n}^+ \bar{T}_{m,p}^+\} = \alpha_n \delta_{np}, \\ \sum_{m=-r}^{s} \alpha_m \{R_{m,n}^- \bar{T}_{m,p}^+ + T_{m,n}^- \bar{R}_{m,p}^+\} &= \sum_{m=-r}^{s} \alpha_m \{R_{m,n}^+ \bar{T}_{m,p}^- + T_{m,n}^+ \bar{R}_{m,p}^-\} = 0, \end{aligned}\right\} \tag{4.10}$$

for $n, p = -r, \ldots, s$. This set of $4M^2$ identities is the counterpart for the present multi-mode problem of that obtained for the general two-dimensional single-mode scattering problem by Kreisel (1949). The identities can be condensed into the single matrix relationship

$$\mathscr{S}^* \mathscr{E} \mathscr{S} = \mathscr{E}, \quad \mathscr{E} = \begin{pmatrix} e & 0 \\ 0 & e \end{pmatrix}, \quad e = \mathrm{diag}\{\alpha_{-r}, \ldots, \alpha_s\}, \tag{4.11}$$

where $\mathscr{S}^* = \bar{\mathscr{S}}^T$ is the hermitian transpose of $\mathscr{S}$. It follows at once that $\mathscr{S}\mathscr{E}^{-1}\mathscr{S}^* =$

$\boldsymbol{\mathcal{E}}^{-1}$. Therefore, the scattering matrix $\hat{\boldsymbol{\mathcal{S}}} = \boldsymbol{\mathcal{E}}^{1/2}\boldsymbol{\mathcal{S}}\boldsymbol{\mathcal{E}}^{-1/2}$ corresponding to a formulation in which the mth wave mode is scaled by $\alpha_m^{1/2}$ throughout is unitary, satisfying $\hat{\boldsymbol{\mathcal{S}}}^*\hat{\boldsymbol{\mathcal{S}}} = \hat{\boldsymbol{\mathcal{S}}}\hat{\boldsymbol{\mathcal{S}}}^* = \boldsymbol{I}$.

It follows from (4.9) that the transfer matrix also satisfies a similarity relation, namely

$$\boldsymbol{\mathcal{P}}^*\boldsymbol{\mathcal{F}}\boldsymbol{\mathcal{P}} = \boldsymbol{\mathcal{F}}, \quad \boldsymbol{\mathcal{F}} = \begin{pmatrix} e & 0 \\ 0 & -e \end{pmatrix}. \tag{4.12}$$

However, unlike $\boldsymbol{\mathcal{S}}$, $\boldsymbol{\mathcal{P}}$ is not similar to a unitary matrix. We note that $|\det(\boldsymbol{\mathcal{S}})| = |\det(\boldsymbol{\mathcal{P}})| = 1$ are immediate consequences of the respective similarity relations and that $|\det(\boldsymbol{T}_-)| = |\det(\boldsymbol{T}_+)|$ and $|\det(\boldsymbol{R}_-)| = |\det(\boldsymbol{R}_+)|$ can be deduced from (4.11).

If there is symmetry in the topography further identities can be derived. Thus, for a bedform which is symmetric about $x = 0$, $\boldsymbol{R}_- = \boldsymbol{R}_+$ and $\boldsymbol{T}_- = \boldsymbol{T}_+$. For a bedform symmetric about $y = 0$, $\boldsymbol{\mathcal{S}}^T = \boldsymbol{\mathcal{E}}\boldsymbol{\mathcal{S}}\boldsymbol{\mathcal{E}}^{-1}$ which implies that $\boldsymbol{R}_\pm^T = e\boldsymbol{R}_\pm e^{-1}$ and $\boldsymbol{T}_\pm^T = e\boldsymbol{T}_\mp e^{-1}$. It follows in particular that $\det(\boldsymbol{\mathcal{P}}) = 1$ for either symmetry.

When the topography is not symmetric, further information about the scattering matrix can be derived in the following way. The formulation holds for any incident angle $\theta_0 \in (-\pi/2, \pi/2)$ and hence for any $\beta_0 \in (-k_0, k_0)$. It can be repeated with $-\beta_0$ in place of β_0, the principal consequences of this change being that $-\beta_{-m}$, α_{-m}, s and r replace β_m, α_m, r and s, respectively. Pursuing this alternative formulation and writing the scattering matrix defined in (4.7) as $\boldsymbol{\mathcal{S}}(\theta_0)$, we find that

$$\overline{\boldsymbol{\mathcal{S}}(\theta_0)}\,\boldsymbol{\mathcal{U}}\,\boldsymbol{\mathcal{S}}(-\theta_0) = \boldsymbol{\mathcal{U}}, \quad \boldsymbol{\mathcal{U}} = \begin{pmatrix} u & 0 \\ 0 & u \end{pmatrix}, \quad u = \{\delta_{m,M+1-n}\}. \tag{4.13}$$

This identity is also of the Kreisel type in that it relates the scattered fields of two different incident waves. When the topography is symmetric about $y = 0$, $\boldsymbol{\mathcal{S}}(\theta_0) = \boldsymbol{\mathcal{U}}\boldsymbol{\mathcal{S}}(-\theta_0)\boldsymbol{\mathcal{U}}$ and (4.13) reduces to $\overline{\boldsymbol{\mathcal{S}}(\theta_0)}\,\boldsymbol{\mathcal{S}}(\theta_0) = I$. For a normally incident wave ($\theta_0 = 0$) and single mode scattering ($k_0 d < \pi$), this reduces further to $\overline{\boldsymbol{\mathcal{S}}(0)}\boldsymbol{\mathcal{S}}(0) = I$, which holds for two-dimensional scattering (see Porter & Chamberlain 1997). In this special case (4.11) also represents the original Kreisel relations.

4.2. *Integral equations*

To evaluate the far-field scattered wave amplitudes, we must first determine $\psi_n^\pm$. If the identity (2.29) is used again, this time with $U = \psi_n^\pm$ and $V = G$, the Green's function satisfying (2.21) and, in the present case, (2.25), we obtain

$$\psi_n^\pm(x, y) = \mathrm{e}^{\mp \mathrm{i}\alpha_n x + \mathrm{i}\beta_n y} - \iint_{S_h} G(x, y|\xi, \eta)\ell(\xi, \eta)\psi_n^\pm(\xi, \eta)\,\mathrm{d}\xi\,\mathrm{d}\eta, \tag{4.14}$$

for all $(x, y) \in S$ and $n = -r, \ldots, s$, where ℓ is defined by (3.5). The equation (4.14) has the same dual rôle as (3.4).

By evaluating (4.14) as $x \to \pm\infty$ and using the appropriate far-field form (2.25) together with (4.4) and (4.5), we deduce that

$$\left.\begin{aligned} 4\mathrm{i}d\alpha_m R_{m,n}^\pm &= -\iint_{S_h} \exp(\mp \mathrm{i}\alpha_m\xi - \mathrm{i}\beta_m\eta)\ell(\xi, \eta)\psi_n^\pm(\xi, \eta)\,\mathrm{d}\xi\,\mathrm{d}\eta, \\ 4\mathrm{i}d\alpha_m\{T_{m,n}^\pm - \delta_{mn}\} &= -\iint_{S_h} \exp(\pm \mathrm{i}\alpha_m\xi - \mathrm{i}\beta_m\eta)\ell(\xi, \eta)\psi_n^\pm(\xi, \eta)\,\mathrm{d}\xi\,\mathrm{d}\eta, \end{aligned}\right\} \tag{4.15}$$

for $m, n = -r, \ldots, s$.

We remark that (4.14) and (4.15) may be used to provide an alternative derivation of the identities (4.10).

4.3. *Numerical method and results*

For a given incident wavenumber, k_0, and angle, θ_0, the scattering matrix $\mathscr{S}$ contains all the information about the scattering properties of the periodic topography, from which all reflected and transmitted modes can be found. The entries of $\mathscr{S}$ are provided by elements $R^{\pm}_{m,n}$, $T^{\pm}_{m,n}$ which are related to the solution $\psi^{\pm}_n(x, y)$, $(x, y) \in S_h$ by the integral relations in (4.15). The function $\psi^{\pm}_n$ itself is determined over S_h from the solution of the integral equation (4.14). The numerical approximation to the solution of this integral equation follows in precisely the manner already described for the determination of Rayleigh–Bloch waves in § 3. Following that procedure here, assuming for simplicity that $S_h \equiv S_{ab}$, leads to the discrete system

$$\psi^{\pm}_n(\boldsymbol{x}_j) + \frac{4ab}{N_x N_y} \sum_{i=1}^{N_x N_y} G_{ij} \ell(\boldsymbol{x}_i) \psi^{\pm}_n(\boldsymbol{x}_i) = \exp\left(\mathrm{i}(\mp\alpha_n, \beta_n) \cdot \boldsymbol{x}_j\right), \quad j = 1, \ldots, N_x N_y, \tag{4.16}$$

for $n = -r, \ldots, s$, where the exponent in the right-hand side is to be interpreted as a scalar product and $\boldsymbol{x}_i$, G_{ij} are given by (3.8) and (3.11) respectively. See the discussion surrounding the discretization in § 3 for details.

Once $\psi^{\pm}_n(\boldsymbol{x}_i)$ has been determined from (4.16) the reflection and transmission coefficients may be approximated by the discretized form of (4.15), namely

$$\left.\begin{aligned} 4\mathrm{i}d\alpha_m R^{\pm}_{m,n} &= -\frac{4ab}{N_x N_y} \sum_{i=1}^{N_x N_y} \exp\left(-\mathrm{i}(\pm\alpha_m, \beta_m) \cdot \boldsymbol{x}_i\right) \ell(\boldsymbol{x}_i) \psi^{\pm}_n(\boldsymbol{x}_i), \\ 4\mathrm{i}d\alpha_m \{T^{\pm}_{m,n} - \delta_{mn}\} &= -\frac{4ab}{N_x N_y} \sum_{i=1}^{N_x N_y} \exp\left(-\mathrm{i}(\mp\alpha_m, \beta_m) \cdot \boldsymbol{x}_i\right) \ell(\boldsymbol{x}_i) \psi^{\pm}_n(\boldsymbol{x}_i), \end{aligned}\right\} \tag{4.17}$$

for $m, n = -r, \ldots, s$.

The solution of (4.16) is obtained easily using an LU matrix solver for $2M$ multiple right-hand sides (each corresponding to a different value of n with both $\pm$ superscripts). Thus, we see that there is little extra effort in determining all $2M$ scattering modes, and hence $\mathscr{S}$, once one sets out to determine just one, the major computational effort being in the generation of the matrix elements. In practice, we are concerned with finding the reflected and transmitted wave amplitude due to a single wave of wavenumber k_0 incident from $x = +\infty$ and making an angle of θ_0 to the x-axis. Thus, we have $A^-_m = 0$ for $m = -r, \ldots, s$ and $A^+_m = \delta_{m0}$, $m = -r, \ldots, s$. The resulting outgoing wave amplitudes given by $\mathbf{B}^{\pm}$ using the scattering matrix, (4.7), we then denote by $R_m = B^+_m$, $T_m = B^-_m$ for $m = -r, \ldots, s$. In this case, the reflected and transmitted wave amplitudes from a single incident wave are related to elements of the scattering matrix by $R_m \equiv R^+_{m,0}$ and $T_m \equiv T^+_{m,0}$.

Let us first consider the convergence of the numerical scheme, already found to be excellent over a whole range of parameters in the trapping problem. Again, convergence of the elements of $\mathscr{S}$ is comparable to that reported in table 1 for the trapping problem provided $k_0 a \gtrsim \frac{1}{2}$. As $k_0 a$ approaches zero, the wavelength becomes long in comparison with the length of the topography and an increase in N_x and N_y is needed to improve numerical results. The known behaviour as $k_0 a \to 0$ is $|R_0| \to 0$, $|T_0| \to 1$. As in the trapping problem of § 3, we choose $N_x = [16a/d]$, $N_y = 16$.

The scattering matrix approach that has been formulated ensures that numerical results automatically satisfy the multi-mode version of the Kreisel relations, amongst them conservation of energy. These relations therefore do not serve as indications of accuracy of the numerical solutions.

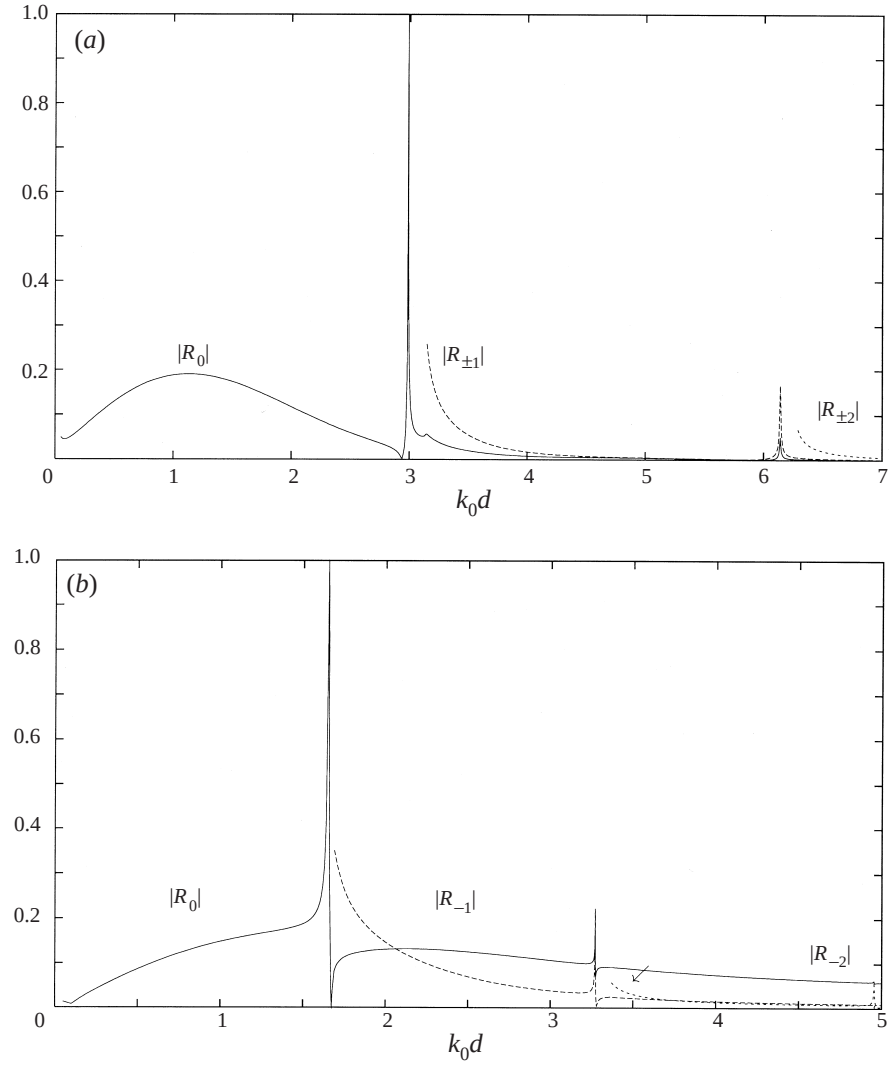

FIGURE 7. Reflection coefficient, $|R_0|$, against k_0d for the bed elevation (3.13) with $a/d = 1$, $b/d = 1$, $d/h_0 = 1$, $A_+ = \frac{1}{2}$. (*a*) $\theta_0 = 0°$, (*b*) $\theta_0 = 60°$.

Figure 7 shows the variation of the modulus of reflection coefficients for the various modes with wavenumber k_0d using the bed elevation defined by (3.13) for incident wave angles of (*a*) $\theta_0 = 0°$ and (*b*) $\theta_0 = 60°$. These curves are typical of the results obtained for other bed elevations. For k_0 small enough, there exists only the fundamental scattered waves, and as k_0 increases through successive cut-offs, further modes appear. The results are much as one might expect, except for one remarkable feature: an isolated peak where $|R_0| = 1$ occurs at a particular value of k_0d just below the first cut-off for the scattering problem. Extensive numerical experimentation reveals that this feature, clearly apparent in both figures 7(*a*) and 7(*b*), is exhibited in the scattering by *any* submerged three-dimensional periodic topography, including unsymmetric bed elevations. As the strip of topography increases in breadth (increasing a/d), further peaks where $|R_0| = 1$ appear for other values of k_0d, all below

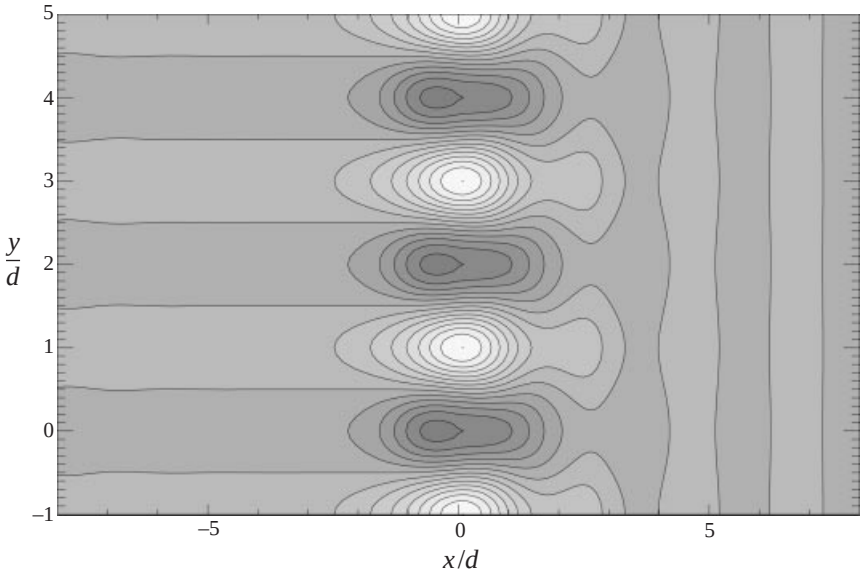

FIGURE 8. A snapshot of the free surface showing total reflection of waves normally incident from $x > 0$ by the bed elevation (3.13): $kd = 2.98836$, $a/d = 1$, $d/h_0 = 2$, $A_+ = \frac{3}{4}$ and $\theta_0 = 0°$.

the first cut-off for the scattering problem. The smaller spikes in the reflected modes just below higher cut-offs peak at values well below unity. Whereas zeros of reflection coefficients are commonplace in scattering by submerged topography, to the authors' knowledge, this example represents the first instance of a zero of transmission, albeit using the mild-slope approximation to the full solution. Indeed, zeros of reflection seem to be closely associated with total reflection, although figures 7(*a*) and 7(*b*) show that the order in which $|R_0| = 1$ and $|R_0| = 0$ occur as a function of wavenumber is not fixed.

It should be emphasized that this phenomenon is not an example of Bragg resonance, where total reflection is the result of interactions over a multiplicity of ripples. Here we are considering only a single element of topography in $|x| \leqslant a$, $|y| \leqslant d$. Further, in the case $\theta_0 = 0$ of normal incidence, boundaries on which a Neumann condition holds may be inserted at $y = \pm d$. We have therefore shown that total reflection can be obtained from topography in a channel with perfectly reflecting walls.

In order to investigate this phenomenon of total reflection further, and to provide some insight into how it is caused, figure 8 shows a snapshot of the free surface at the frequency $k_0 d = 2.98836$ at which total reflection occurs in the normally incident case corresponding to figure 7(*a*). Three periods of topography occur in the y/d-direction within the strip $-1 \leqslant x/d \leqslant 1$ and the wave is incident from the right. The contours on the far left of figure 8 correspond to zero free surface elevation and are not able to show that the wave amplitude actually decays very rapidly to zero as $x/d \to -\infty$. In contrast, the wave amplification over the topography is relatively high (of the order of 10 times the incident wave height). One must be careful when predicting such large amplifications using linearized theory, as nonlinear effects will undoubtably play an important rôle in these instances. Such a situation suggests the influence of a trapped mode – or a nearly trapped mode – over the topography, so we return to the trapping problem of § 3, but now seek Rayleigh–Bloch modes satisfying the

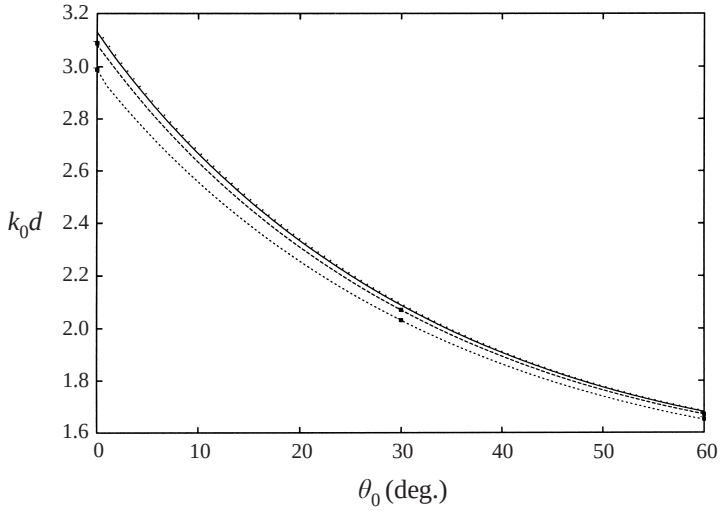

FIGURE 9. Variation of near-trapping wavenumbers with angle of incidence θ for the bed elevation (3.13) with $a/d = 1$, $b/d = 1$, $d/h_0 = 1$, $A_+ = \frac{1}{4}, \frac{1}{2}, \frac{3}{4}$. The dotted line denotes the first cut-off and the symbols the zeros of transmission in the corresponding scattering problem.

relation $\beta = k_0 \sin\theta_0$. That is, $k_0 > \beta$, above the cut-off for the trapping problem. It is found that, in general, no Rayleigh–Bloch solutions are obtained above the cut-off, although we do not rule out the possibility that they may exist for certain specific geometries. However, we do find that there exist *nearly trapped* Rayleigh–Bloch solutions corresponding exactly to the wavenumbers at which total reflection occurs in the scattering problem. A nearly trapped mode is one in which, instead of the operator KL having a real eigenvalue equal to unity for a real value of k_0, there is a (complex) eigenvalue very close to unity for a real k_0. Alternatively, the eigenvalue equals unity for a value of k_0 having a very small imaginary part. (We note that for $k_0 > \beta$ the kernel of K is not hermitian and therefore the proof given for the trapping problem that KL has real eigenvalues does not apply.)

Curves of the variation of nearly trapped mode frequencies against incident wave angle for the bed elevation defined by (3.13) at heights $A_+ = \frac{1}{4}, \frac{1}{2}, \frac{3}{4}$ are shown in figure 9, overlaid with selected points showing instances of total reflection in the corresponding scattering problems. The dotted line closely bounding the three curves above represents a measure of the variation of the first cut-off wavenumber for the scattering problem with θ_0.

The presence of a nearly-trapped mode is consistent with the observed near-resonance in the scattering problem, but further work needs to be done to understand why total reflection should occur.

4.4. *Multiple rows of periodic topography: a wide-spacing approximation*

The amount of computational effort required to directly calculate the reflection of waves by multiple rows of topography rapidly increases as the number of rows, all of which must be discretized numerically, increases.

Approximations to the reflected and transmitted wave amplitudes in the scattering of waves by multiple rows of periodic bed topography can be made using the well-known wide-spacing approximation. Let us consider a configuration consisting of N parallel rows of periodic topography, each row having the same period, $2d$. Let the

ith row have width $2a_i$, say, centred on the plane $x = x_i$ $(i = 1, 2, \ldots, N)$ such that $x_1 < x_2 < \ldots < x_N$. It is assumed that the reflection and transmission properties of each of the rows centred about $x = 0$ is known, and we label corresponding transfer matrices $\mathscr{P}_i$, $i = 1, \ldots, N$, using the definition (4.9). We also define

$$w_i = (x_{i+1} - x_i)/(a_{i+1} + a_i), \quad i = 1, \ldots, N-1,$$

so that $w_i \geqslant 1$ represents the spacing between adjacent rows of topography and $w_i = 1$ implies that the ith and $(i+1)$th rows are touching. The wide-spacing approximation, which ignores the effect of evanescent mode interaction between neighbouring rows of topography, is strictly valid for $kw_i \gg 1$, $i = 1, \ldots, N-1$, although it is often used for relatively small separations. Indeed, we shall be using it for $w_i = 1$, that is, for rows that touch. Notice that in the following derivation of the wide-spacing results, no assumption is made about the alignment between topography in adjacent rows.

We concentrate on the wave interactions at the ith row. In the region $x_{i-1} + a_{i-1} < x < x_i - a_i$ let the incoming and outgoing propagating waves be characterized by the wave vectors $\boldsymbol{A}_i^-$ and $\boldsymbol{B}_i^-$ respectively in accordance with the notation used in § 4.1. In $x_i + a_i < x < x_{i+1} - a_{i+1}$ incoming and outgoing propagating waves are represented by the vectors $\boldsymbol{A}_i^+$ and $\boldsymbol{B}_i^+$ respectively. If the ith row were centred on $x = 0$ then (4.8) would give the appropriate transfer. Instead, it needs to be modified to account for the phase shifts in the wave components travelling to the right and left. Thus we have

$$\mathscr{D}_i \begin{pmatrix} \boldsymbol{A}_i^- \\ \boldsymbol{B}_i^- \end{pmatrix} = \mathscr{P}_i \mathscr{D}_i \begin{pmatrix} \boldsymbol{B}_i^+ \\ \boldsymbol{A}_i^+ \end{pmatrix}, \tag{4.18}$$

where

$$\mathscr{D}_i = \begin{pmatrix} \bar{d}_i & 0 \\ 0 & d_i \end{pmatrix}, \quad d_i = \operatorname{diag}\{\mathrm{e}^{\mathrm{i}\alpha_n x_i}\}_{n=-r,\ldots,s}, \quad i = 1, \ldots, N. \tag{4.19}$$

Note that $\mathscr{D}_i^{-1} = \bar{\mathscr{D}}_i$. Since the wave field to the right of the row centred on $x = x_i$ is the same as that to the left of the row centred on $x = x_{i+1}$ it is clear that

$$\begin{pmatrix} \boldsymbol{B}_i^+ \\ \boldsymbol{A}_i^+ \end{pmatrix} = \begin{pmatrix} \boldsymbol{A}_{i+1}^- \\ \boldsymbol{B}_{i+1}^- \end{pmatrix},$$

and so (4.18) may be applied successively from $i = 1$ to $i = N$ to give

$$\begin{pmatrix} \boldsymbol{A}_1^- \\ \boldsymbol{B}_1^- \end{pmatrix} = \mathscr{Q} \begin{pmatrix} \boldsymbol{B}_N^+ \\ \boldsymbol{A}_N^+ \end{pmatrix}, \tag{4.20}$$

where

$$\mathscr{Q} = \bar{\mathscr{D}}_1 \mathscr{P}_1 \mathscr{D}_1 \bar{\mathscr{D}}_2 \mathscr{P}_2 \mathscr{D}_2 \ldots \bar{\mathscr{D}}_N \mathscr{P}_N \mathscr{D}_N \equiv \begin{pmatrix} Q_{11} & Q_{12} \\ Q_{21} & Q_{22} \end{pmatrix}, \tag{4.21}$$

say, Q_{ij}, $i, j = 1, 2$, being $M \times M$ matrices. In (4.20) the vectors $\boldsymbol{A}_1^-$, $\boldsymbol{B}_1^-$ contain the amplitudes in $-\infty < x < x_1 - a_1$ of the wave modes travelling to the right and left respectively whilst $\boldsymbol{B}_N^+$, $\boldsymbol{A}_N^+$ contain wave modes in $x_N + a_N < x < \infty$ associated with waves travelling to the right and left respectively.

In the same manner as in § 4.1 we can consider $2M$ scattering problems for this N-row wide-spacing formulation, with the far-field behaviour given by (4.4) and (4.5) for waves incident from $x = -\infty$ and $x = +\infty$ respectively. Applying (4.20) to each

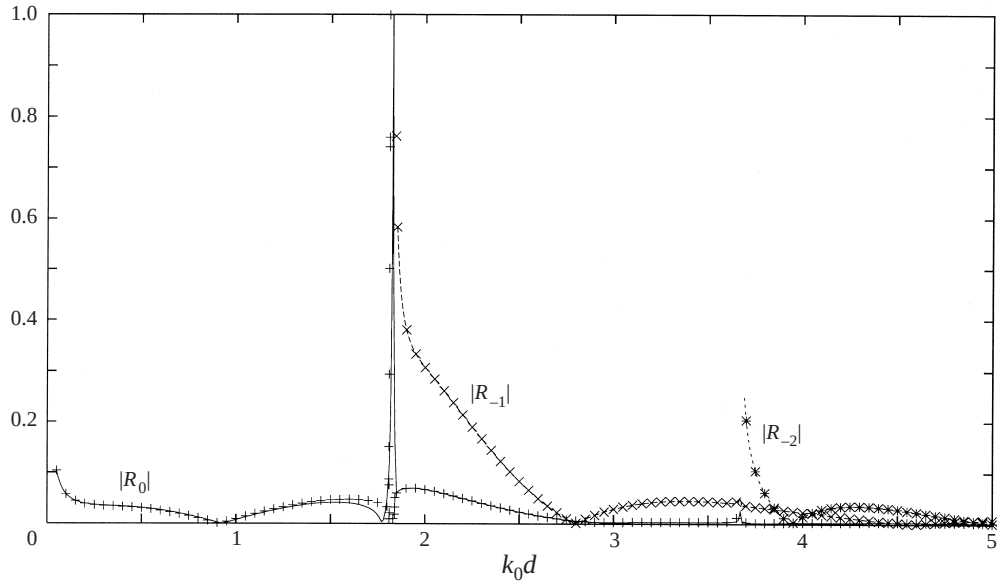

FIGURE 10. Comparison between reflection coefficients from direct calculation (symbols) and wide-spacing approximation (lines) for two touching rows of topography defined by (3.13) with $A_+ = \frac{3}{4}$, $d/h_0 = 1$, $a/d = 1$, $b/d = 1$, $\theta_0 = 45°$.

of these scattering problems and manipulating results in the scattering matrix

$$\mathscr{S} = \begin{pmatrix} Q_{21}Q_{11}^{-1} & Q_{22} - Q_{21}Q_{11}^{-1}Q_{12} \\ Q_{11}^{-1} & -Q_{11}^{-1}Q_{12} \end{pmatrix}, \tag{4.22}$$

from which the reflection and transmission matrices may be identified using (4.7).

Figure 10 compares the wide-spacing approximation with a direct calculation for two touching rows of periodic topography ($w_1 = 1$) defined by (3.13). The agreement is excellent everywhere except close to the point at which total reflection occurs. This disparity is to be expected since we have already seen in figure 8 that the wave amplitude at total reflection is large and so we would expect strong interaction of evanescent modes near this wavenumber. We will now use the wide-spacing approximation to investigate the effect of Bragg resonance, and will not be concerned with accurately estimating the reflection around the peak $|R_0| = 1$.

4.5. *Bragg resonance for multiple rows of topography*

In *two-dimensional* scattering of waves by several periods of topography Bragg resonance is a well-established phenomenon (see, for example, Chamberlain & Porter 1995). Here, we investigate the possibility of generating Bragg resonance over multiple rows of three-dimensional periodic topography.

For multiple identical rows of topography that are equally spaced, we let $a_i \equiv a$, $\mathscr{P}_i \equiv \mathscr{P}$ and $x_i = i\ell$, $i = 1, \ldots, N$. Then from (4.21) $\mathscr{Q}$ simplifies to

$$\mathscr{Q} = (\mathscr{A}\mathscr{P})^N \mathscr{D}_N, \quad \mathscr{A} = \begin{pmatrix} \delta & 0 \\ 0 & \bar{\delta} \end{pmatrix}, \quad \delta = \operatorname{diag}\{e^{i\alpha_n \ell}\}_{n=-r,\ldots,s}. \tag{4.23}$$

The effect of a multiplicity of identical rows on the scattering process can therefore

be investigated by using the spectral decomposition of the phase-modified transfer function $\boldsymbol{\Delta}\boldsymbol{\mathscr{P}}$ for one row. Since $\boldsymbol{\Delta}$ is a unitary matrix, it follows from (4.12) that $(\boldsymbol{\Delta}\boldsymbol{\mathscr{P}})^*\boldsymbol{\mathscr{F}}(\boldsymbol{\Delta}\boldsymbol{\mathscr{P}}) = \boldsymbol{\mathscr{F}}$ so that $\boldsymbol{\Delta}\boldsymbol{\mathscr{P}}$ and $(\boldsymbol{\Delta}\boldsymbol{\mathscr{P}})^{*-1}$ are similar matrices. Therefore, if λ_i is an eigenvalue of $\boldsymbol{\Delta}\boldsymbol{\mathscr{P}}$ then so is $\overline{\lambda_i}^{-1}$ and the eigenvalues of $\boldsymbol{\Delta}\boldsymbol{\mathscr{P}}$ either occur in distinct (real or complex) pairs with reciprocal magnitudes or have unit magnitude. We noted after (4.12) that if the topography is symmetric about $x = 0$ or $y = 0$, or both, then $\det(\boldsymbol{\mathscr{P}}) = 1$ implying that $\det(\boldsymbol{\Delta}\boldsymbol{\mathscr{P}}) = 1$. We infer the additional information for symmetric topography that the complex eigenvalues of $\boldsymbol{\Delta}\boldsymbol{\mathscr{P}}$ occur in conjugate pairs.

Excluding exceptional cases where the parameters are such that the eigenvalues of $\boldsymbol{\Delta}\boldsymbol{\mathscr{P}}$ coincide, there exists a non-singular matrix $\mathbf{C}$, the columns of which are the eigenvectors of $\boldsymbol{\Delta}\boldsymbol{\mathscr{P}}$, such that

$$\boldsymbol{\Delta}\boldsymbol{\mathscr{P}} = \mathbf{C}\boldsymbol{\Lambda}\mathbf{C}^{-1},$$

where $\boldsymbol{\Lambda}$ is the diagonal matrix of eigenvalues of $\boldsymbol{\Delta}\boldsymbol{\mathscr{P}}$. Therefore from (4.23)

$$\mathscr{Q} = \mathbf{C}\boldsymbol{\Lambda}^N\mathbf{C}^{-1}D_N \tag{4.24}$$

is the overall transfer matrix for the topography. From this it is clear that an eigenvalue of $\boldsymbol{\Delta}\boldsymbol{\mathscr{P}}$ which has magnitude greater than unity leads to an amplification in components of $\mathscr{Q}$ as N increases.

The effect of this amplification can readily be determined in the single mode ($M = 1$) case in which $\mathscr{Q}$ is a 2×2 matrix and $\boldsymbol{\Delta}\boldsymbol{\mathscr{P}}$ has eigenvalues λ and $\bar{\lambda}^{-1}$, say. It is found that

$$R_- = (|\lambda|^{2N} - 1)c_{21}c_{22}/(|\lambda|^{2N}c_{11}c_{22} - c_{12}c_{21}),$$
$$T_- = \lambda^N \mathrm{e}^{\mathrm{i}\alpha_0 x_N}/(|\lambda|^{2N}c_{11}c_{22} - c_{12}c_{21}),$$

with $\mathbf{C} = \{c_{ij}\}$. If $|\lambda| > 1$ then $|R_-| \to |c_{21}/c_{11}|$ and $|T_-| \to 0$ as $N \to \infty$. Since $|R_-|^2 + |T_-|^2 = 1$ follows from (4.10) in this case, we actually have $|R_-| \to 1$. (An examination of the eigenvalue problem for $\boldsymbol{\Delta}\boldsymbol{\mathscr{P}}$ confirms that $|c_{11}| = |c_{21}|$.)

Thus eigenvalues of $\boldsymbol{\Delta}\boldsymbol{\mathscr{P}}$ having magnitude greater than unity are associated with Bragg resonance, at least in the case $M = 1$. Adopting a similar approach to multi-mode scattering does not provide such a transparent relationship between the eigenvalues of $\boldsymbol{\Delta}\boldsymbol{\mathscr{P}}$ and the scattered wave amplitudes. Even so, it seems likely that an eigenvalue for which $|\lambda_i| \neq 1$ will be an indicator of resonance and this connection can be explored numerically.

In two-dimensional (single mode) scattering it is well-known that Bragg resonance occurs over periodic topography if the incident wavelength is double the periodicity. On this basis, resonance would be expected in the nth mode ($n = -r, \ldots, s$) where $\alpha_n \ell = p\pi$, ℓ being the periodicity of the topography in the x-direction. Additional resonances resulting from interactions between modes are also possible.

In figure 11(a) we show the modulus of the reflected modes computed using the wide-spacing formulation for $N = 8$ identical rows of topography each described by (3.13) with $a/d = 1$, $b/d = 1$, $d/h_0 = 2$, $A_+ = \frac{1}{2}$ and for an incident wave angle of $\theta_0 = 30°$. The spacing is $\ell/d = 2$ such that the adjacent rows touch and reference to the results observed in figure 9 means that we do not expect to accurately predict the reflection coefficient close to the first cut-off. In figure 11(b) the modulus of those eigenvalues of the matrix $\boldsymbol{\Delta}\boldsymbol{\mathscr{P}}$ such that $0 < |\lambda_i| \leqslant 1$ are plotted (since eigenvalues occur in pairs, λ_i and $1/\lambda_j$, for each eigenvalue $|\lambda_i| < 1$ there is a corresponding eigenvalue with modulus $1/|\lambda_i|$).

Apart from the narrow peak in the modulus reflection coefficient, $|R_0| = 1$, occurring just below the first cut-off, already shown to be associated with a nearly trapped

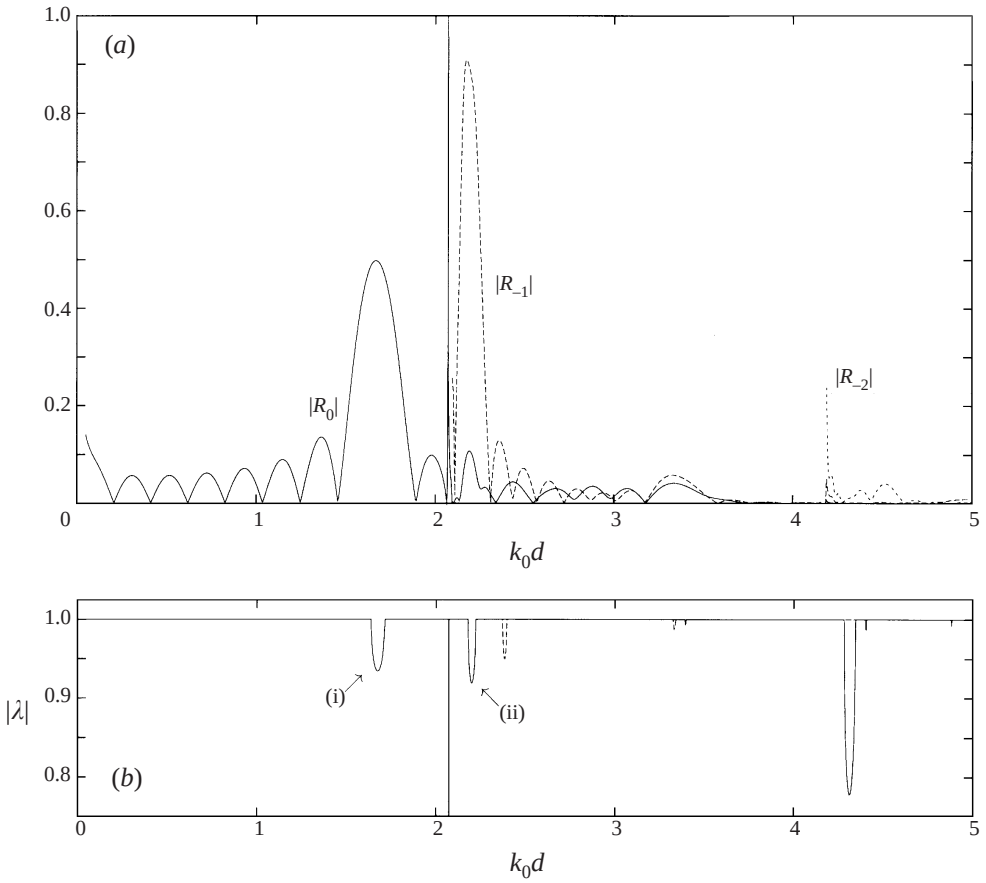

FIGURE 11. (*a*) Reflected amplitudes against k_0d for eight touching strips of topography each defined by (3.13) with $a/d = 1$, $d/h_0 = 2$, $b/d = 1$, $A_+ = 0.5$ and for an incident wave angle of $\theta_0 = 30°$. (*b*) Modulus of eigenvalues of $\boldsymbol{\Delta\mathscr{P}}$ against k_0d for those eigenvalues with $|\lambda| \leqslant 1$.

wave, there are two broader peaks in the modulus of the reflection coefficients clearly visible in figure 11(*a*). The first peak, with $|R_0| \approx 0.5$, below the first cut-off, occurs at wavenumber component in the x-direction, $\alpha_0\ell \equiv k_0\ell\cos\theta_0$, just below a value of π, a result entirely consistent with the single mode scattering by two-dimensional periodic topography. The resonance is indicated by the pair of eigenvalues of the matrix $\boldsymbol{\Delta\mathscr{P}}$ of reciprocal modulus making a brief excursion from unit modulus over a small interval of wavenumber. Only the eigenvalue having modulus less than or equal to unity is shown in figure 11(*b*) and labelled by (i). The second prominent peak in the modulus of a reflection coefficient occurs after the first cut-off in the second reflected mode, R_{-1}, to a value of approximately 0.9. This resonance is indicated in figure 11(*b*) by an eigenvalue of $\boldsymbol{\Delta\mathscr{P}}$ associated with the mode R_{-1} whose modulus moves away from unity over an interval of wavenumber, labelled (ii). In this case, the modulus of the eigenvalues associated with the first reflected mode, R_0, also follow those of the mode R_{-1}. Thus one might expect to observe large peaks in both $|R_0|$ and $|R_{-1}|$, instead of just the latter mode. In fact, increasing N, the number of rows of periodic topography, does amplify the small peak in $|R_0|$ just visible in figure 11(*a*). There are further fluctuations in eigenvalue modulus for larger values of k_0d, although

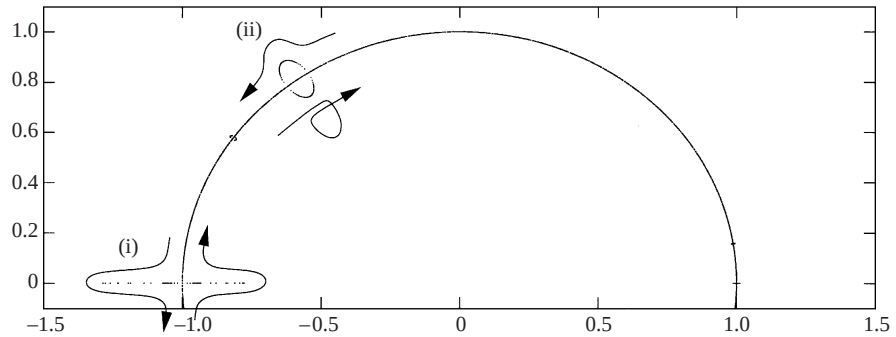

FIGURE 12. The trace of the eigenvalues in the complex plane for $0 < k_0 d < 5$ corresponding to the results in figure 11. The arrows indicate the path two eigenvalues take as they meet on the unit circle.

these do not appear have such a strong influence on the reflection coefficients in the corresponding modes. Increasing the value of N does, however, pick out amplification in the reflection in those modes.

In addition to showing the modulus of the eigenvalues as a function of wavenumber, it is instructive to examine the path of the eigenvalues in the complex plane as the wavenumber is increased. Thus, in figure 12, the path of the eigenvalues corresponding to the results in figure 11 are shown for $0 < k_0 d \leqslant 5$. Since the topography is symmetric about the planes $x = 0$ and $y = 0$, eigenvalues occur in complex-conjugate pairs and so only the upper half-plane is shown. Resonance coincides with eigenvalues moving off the unit circle. The mechanism by which this happens can be gathered from figure 12, the arrows indicating the path which the eigenvalues take. Thus, eigenvalues traversing the unit circle in opposite directions do not simply pass through one another as $k_0 d$ is varied. Instead, as they coalesce, they move off the unit circle in opposite directions before returning to the unit circle and continuing in their original direction. For the particular example we are considering, the resonance indicated by the peak labelled (i) in figure 11(b), a pair of complex-conjugate eigenvalues meet at $\lambda_i = -1$. As previously mentioned, this resonance may be regarded as the direct analogue of the Bragg resonance in single mode scattering, occurring at a value of $\alpha_n = \pi/l$, and associated with wave coupling with the bed periodicity. The resonance labelled (ii) in figure 11 occurs when two eigenvalues associated with *different* scattered modes, traversing the unit circle in opposite direction, meet as indicated by (ii) in figure 12. Here, it appears that a more complicated coupling is occurring between the bed periodicity and a pair of distinct scattering modes. By examining the onset of resonance for small-amplitude bed elevations, it can be confirmed numerically that the condition for this type of resonance is

$$\alpha_n + \alpha_m = 2\pi/\ell, \quad -r \leqslant n, m \leqslant s, \tag{4.25}$$

whilst for larger-amplitude bed elevations, this condition is only approximately satisfied. It is beyond the scope of the present paper to investigate the relation (4.25) analytically and this will form the subject of another paper. Setting n equal to m allows the relation (4.25) to encapsulate the single mode resonance condition.

Figures 13(a, b) shows the modulus of reflection coefficients and variation of $|\lambda_i|$ with wavenumber for the same geometrical configuration as that in figure 11, but with the incident wave angle increased from $\theta_0 = 30^\circ$ to $\theta_0 = 60^\circ$. This change has the effect of shifting the resonant peak in R_0 given by the condition $\alpha_0 \approx \pi/\ell$ beyond the

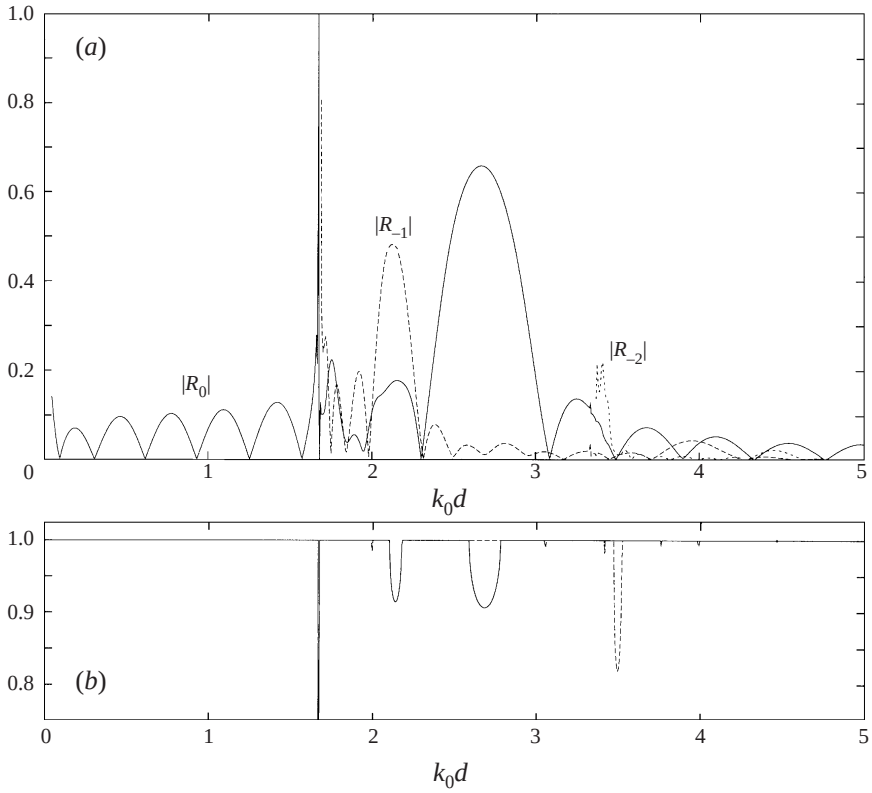

FIGURE 13. (*a*) Modulus of reflection coefficients against k_0d for eight touching strips of topography each defined by (3.13) with $a/d = 1$, $d/h_0 = 2$, $b/d = 1$, $A_+ = 0.5$ and for an incident wave angle of $\theta_0 = 45°$. (*b*) Modulus of eigenvalues of $\boldsymbol{\Delta}\boldsymbol{\mathscr{P}}$ against k_0d for those eigenvalues with $|\lambda_i| \leqslant 1$.

first cut-off. There is now a less significant peak in the R_{-1} mode associated with the resonant condition $\alpha_0 + \alpha_{-1} = 2\pi/\ell$, despite a more discernible peak in the $|R_0|$ over the same interval of wavenumber, where the eigenvalues suggest resonance should occur in both modes (see figure 13(*b*)).

Further numerical experimentation suggests that the two most significant contributions to resonance in reflected modes coincide with the condition $\alpha_0 = \pi/\ell$ in the fundamental mode and with $\alpha_0 + \alpha_{-1} = 2\pi/\ell$, the first instance of interaction between the first two scattered modes and the bed periodicity.

5. Conclusions

The work described in this paper was conceived with two principal aims. The first of these is to examine whether trapped Rayleigh–Bloch waves, which are known to exist in the presence of an infinite array of vertical cylinders, for example, can also propagate over an infinite array of periodic topography. The second is to investigate the phenomenon of Bragg resonance, familiar in the setting of two-dimensional water wave scattering by periodic bed formations, in the three-dimensional context.

Both aims are served by considering wave motions over a doubly modulated bedform which extends to infinity in one direction, a basic requirement of the trapping

problem, and is of finite extent in the orthogonal horizontal direction, allowing the scattering problem to be formulated.

Three-dimensional water wave problems involving bed irregularities have received almost no attention using full-linear theory, not least because they are computationally expensive to resolve. We have overcome this difficulty to some extent by reducing the dimension of the problem using the modified mild-slope equation, which gives good approximations in the corresponding two-dimensional context. This approach has made it possible to carry out a thorough investigation and identify areas in which full-linear theory may, perhaps, be attempted on a limited scale.

The two main objectives have been realized and a number of new phenomena have also been discovered. It has been shown that Rayleigh–Bloch waves can exist over a periodically repeating bed shape of infinite extent, provided that enough of that shape is elevated above the prevailing bed level. By introducing parallel vertical walls to isolate a finite number of cycles of the topography, the results may be interpreted in relation to motion in a channel. In this context, wave trapping over localized topography is found to be possible under less restrictive conditions than those required in the corresponding case of vertical cylinders.

For the scattering problem, we have shown that Bragg resonance does arise over doubly periodic ripple beds. Indeed, the multiplicity of travelling wave modes permitted in the three-dimensional setting leads to a corresponding multiplicity in the occurrences of resonance. Thus, a prescribed incident wave in one mode can induce significant reflection in another mode, having a different wavelength and a direction different from that given by Snell's law.

A more surprising outcome of the investigation into scattering is the existence of total reflection from a single row of periodic topography, in both the general problem and the particular case in which there is a localized bed elevation in a parallel-sided channel. This scattering phenomenon, which is quite distinct from the multiple row interaction leading to Bragg resonance, couples the two main aspects of the work, for it is shown to be closely related to an equally unexpected feature in the trapping problem, namely the existence of a nearly trapped wave in the continuous spectrum.

Appendix. The operator K

The key to the proof that K is a positive operator on $L_2(S_h)$ is the use of the identity

$$\mathrm{e}^{-\gamma_m|x-\xi|} = \frac{2\gamma_m}{\pi}\int_0^\infty \frac{\cos\{t(x-\xi)\}}{t^2+\gamma_m^2}\,\mathrm{d}t,$$

in the representation (2.22) of the kernel $G(x,y|\xi,\eta)$ of K, which gives

$$G(x,y,|\xi,\eta) = \frac{1}{2d\pi}\sum_{m=-\infty}^{\infty}\int_0^\infty \frac{1}{t^2+\gamma_m^2}\{(\overline{\cos(tx)\mathrm{e}^{-\mathrm{i}\beta_m y}})(\cos(t\xi)\mathrm{e}^{-\mathrm{i}\beta_m\eta}).$$
$$+(\overline{\sin(tx)\mathrm{e}^{-\mathrm{i}\beta_m y}})(\sin(t\xi)\mathrm{e}^{-\mathrm{i}\beta_m\eta})\}\,\mathrm{d}t.$$

Therefore, for any $\chi \in L_2(S_h)$,

$$(\mathsf{K}\chi,\chi) = \iint_{S_h}\overline{\chi(x,y)}\iint_{S_h}G(x,y|\xi,\eta)\chi(\xi,\eta)\mathrm{d}\xi\mathrm{d}\eta\,\mathrm{d}x\mathrm{d}y$$
$$= \frac{1}{2d\pi}\sum_{m=-\infty}^{\infty}\int_0^\infty \frac{\{|C_m(t)|^2+|S_m(t)|^2\}}{t^2+\gamma_m^2}\,\mathrm{d}t,$$

where

$$C_m(t) = \iint_{S_h} \cos(tx) e^{-i\beta_m y} \chi(x,y) dx\, dy, \quad S_m(t) = \iint_{S_h} \sin(tx) e^{-i\beta_m y} \chi(x,y) dx\, dy.$$

Therefore $(\mathsf{K}\chi, \chi) \geqslant 0$ and K is a non-negative operator.

Now $(\mathsf{K}\chi, \chi) = 0$ implies that $C_m(t) = S_m(t) = 0$ for all $m \in \mathbb{Z}$ and all $t \geqslant 0$ or, equivalently, that

$$\iint_{S_h} e^{-itx - i\beta_m y} \chi(x,y) dx\, dy = 0$$

for all $m \in \mathbb{Z}$ and all $t \in \mathbb{R}$.

Let S_r denote the rectangular domain in which $-a \leqslant x \leqslant a, -d \leqslant y \leqslant d$, so that $S_h \subseteq S_r$, and define

$$\hat{\chi}(x,y) = \chi(x,y), \quad (x,y) \in S_h,$$
$$= 0, \quad (x,y) \in S_r \backslash S_h.$$

Then $(\mathsf{K}\chi, \chi) = 0$ implies that

$$D_m(t) \equiv \iint_{S_r} e^{-itx - i\beta_m y} \hat{\chi}(x,y) dx\, dy = 0$$

for all $m \in \mathbb{Z}$ and all $t \in \mathbb{R}$. Now every $\hat{\chi} \in L_2(S_r)$ can be written in the form

$$\hat{\chi}(x,y) = \frac{1}{4ad} \sum_{n=-\infty}^{\infty} \sum_{m=-\infty}^{\infty} D_m(n\pi/a) X_n(x) Y_m(y),$$

for almost all $(x,y) \in S_r$, since

$$X_n(x) = e^{inx\pi/a} \ (n \in \mathbb{Z}), \quad Y_m(y) = e^{i\beta_m y} \ (m \in \mathbb{Z}),$$

are complete orthogonal sets on $L_2(-a,a)$ and $L_2(-d,d)$, respectively. We conclude that $\hat{\chi} = 0$, as a member of $L_2(S_r)$, and hence that $(\mathsf{K}\chi, \chi) = 0$ implies that $\chi = 0$.

Therefore $(\mathsf{K}\chi, \chi) > 0$ for all $\chi \in L_2(S_h)$ except $\chi = 0$, and K is a positive operator.

REFERENCES

Berkhoff, J. C. W. 1973 Computation of combined refraction-diffraction *Proc. 13th Conf. Coastal Engng, July 1972, Vancouver*, pp. 471–490. ASCE.

Berkhoff, J. C. W. 1976 Mathematical models for simple harmonic linear waves. Wave diffraction and refraction. PhD thesis, Technical University of Delft.

Chamberlain, P. G. & Porter, D. 1995 The modified mild-slope equation. *J. Fluid Mech.* **291**, 393–407.

Davies, A. G. & Heathershaw, A. D. 1984 Surface-wave propagation over sinusoidally varying topography. *J. Fluid Mech.* **144**, 419–443.

Evans, D. V. & Fernyhough, M. 1995 Edge waves along periodic coastlines. Part 2. *J. Fluid Mech.* **297**, 307–325.

Evans, D. V. & Linton, C. M. 1993 Edge waves along periodic coastlines. *Q. J. Mech. Appl. Maths* **46**, 642–656.

Guazzelli, E., Rey, V. & Belzons, M. 1992 Higher-order Bragg reflection of gravity surface waves by periodic beds. *J. Fluid Mech.* **245**, 301–317.

Kirby, J. T. 1986 A general wave equation for waves over rippled beds. *J. Fluid Mech.* **162**, 171–186.

Kreisel, G. 1949 Surface waves. *Q. Appl. Maths* **7**, 21.

Linton, C. M. 1998 The Green's function for the two-dimensional Helmholtz equation in periodic domains. *J. Eng. Maths* **33**, 377–402.

LINTON, C. M. & EVANS, D. V. 1993 The interaction of waves with a row of circular cylinders. *J. Fluid Mech.* **251**, 687–708.

MANIAR, H. D. & NEWMAN, J. N. 1997 Wave diffraction by a long array of cylinders. *J. Fluid Mech.* **339**, 309–330.

MCIVER, M. & LINTON, C. M. 1995 On the non-existence of trapped modes in acoustic waveguides. *Q. J. Mech. Appl. Maths* **48**, 543-555.

MCIVER, P., LINTON, C. M. & MCIVER, M. 1998 Construction of trapped modes for wave guides and diffraction gratings. *Proc. R. Soc. Lond.* A **48**, 2593–2616.

MEI, C. C. 1985 Resonant reflection of surface water waves by periodic sandbars. *J. Fluid Mech.* **152**, 315–335.

O'HARE, T. J. & DAVIES, A. G. 1992 A new model for surface wave propagation over undulating topography. *Coastal Engng* **18**, 251–266.

PORTER, D. & CHAMBERLAIN, P. G. 1997 Linear wave scattering by two-dimensional topography. In *Gravity Waves in Water of Finite Depth* (ed. J. N. Hunt), pp. 13–53. Computational Mechanics, Southampton.

PORTER, R. & EVANS, D. V. 1999 Rayleigh–Bloch surface waves along periodic gratings and their connection with trapped modes in waveguides. *J. Fluid Mech.* **386**, 233–258.

SMITH, R. & SPRINKS, T. 1975 Scattering of surface waves by a conical island. *J. Fluid Mech.* **72**, 373–384.

UTSUNOMIYA, T. & EATOCK TAYLOR, R. 1999 Trapped modes around a row of circular cylinders in a channel. *J. Fluid Mech.* **386**, 259–279.